A new global database of Mars impact craters ≥1 km: 2. Global crater properties and regional variations of the simple-to-complex transition diameter

Stuart J. Robbins*
Laboratory for Atmospheric and Space Physics; University of Colorado at Boulder, UCB 600, Boulder, CO 80309, United States
stuart.robbins@colorado.edu
*Corresponding Author

Brian M. Hynek
Laboratory for Atmospheric and Space Physics and Department of Geological Sciences; University of Colorado at Boulder, UCB 600, Boulder, CO 80309, United States
hynek@lasp.colorado.edu

Submitted to Journal of Geophysical Research on 20 Sept. 2011
Revision submitted 26 Jan. 2012
Revision 2 submitted 29 Mar. 2012
Revision 3 submitted 20 Apr. 2012

Total Pages - 63; Total Tables - 3; Total Figures - 15.

Running Head: Mars Crater Database: Results

Abstract:

We have generated a new, 384,343-entry global crater database of Mars, statistically complete for craters with diameters $D \geq 1$ km. In this release, the database contains detailed morphologic and morphometric data for craters $D \geq 3$ km (future releases will extend these to smaller diameters). With detailed topographic data for the largest crater database to-date, we analyzed crater depth-to-diameter ratios for simple and complex morphologies across various terrains and for the planet as a whole and investigated the simple-to-complex morphology transition. Our results are similar to those in the published literature, but we found a substantial terrain dependence of the simple-to-complex transition that occurs at ~11-km-diameter craters at high latitudes. This suggests a model that requires melting of volatiles during high-latitude crater formation that fill the crater during the modification phase but will still support the simple morphology to larger diameters. We also use this database to reexamine previously observed distributions and patterns to show its fidelity and to further explore other global relationships of fresh craters, those with central peaks, pits, and summit pits. We present the global distribution of craters with different types of ejecta and morphometric properties. Overall, this database is shown to be comparable to previous databases where there is overlap and to be useful in extending prior work into new regimes.

Keywords: Mars, Mars craters

Index Terms: 6225 Mars; 5420 Impact phenomena, cratering; 6055 Surfaces

1. Introduction

Crater populations can inform a variety of investigations of planetary processes, surface properties, physics, and geology. Detailed investigations of these require data about craters' positions, diameters, depths, and morphologies. Prior detailed work has focused on deriving these for isolated regions of Mars and so a true, global study has not been done with the crater properties that modern data permit to be gathered and derived, though global analyses have been done before [*e.g.*, *Strom et al*., 1992]. To this end, we have compiled the largest planetary crater database that exists today. This Martian crater catalog contains 384,343 craters with diameters $D \geq 1$ km; the primary imagery data source was THEMIS Daytime IR mosaics at 233 m/pix and 100 m/pix scales [*Christensen et al*., 2004; *Edwards et al*., 2011] (CTX imagery [*Malin et al*., 2007] was occasionally used to supplement at high northern latitudes). In a process described in *Robbins and Hynek* [2012], this volume, we classified and derived many dozen morphologic and morphometric descriptors for each crater. Measurements from the database that were used in this work are from THEMIS-based circle fits unless otherwise explicitly stated.

To both illustrate the fidelity and utility of this work, we have reexamined many previous general trends and properties of Martian impact craters reported in the literature and take them to new regimes. The small crater distribution as well as locations of fresh craters are examined in Section 2. Crater interior and ejecta morphology are examined in Section 3, exploring the distribution of crater central peaks, central pits, summit pits, and both radial and cohesive layered ejecta. Section 4 addresses revision of Martian crater topographic properties with the new data; it shows that rim heights are $\sim 2\times$ smaller than are found on the Moon. Sections 5 and 6 present detailed recalculations of the depth-to-diameter function for simple and complex craters and the simple-to-complex morphology transition. This is done globally and by terrain that yielded disparate results discussed in Section 7.

2. Global Crater Distributions

The global crater distribution of Mars is generally well characterized in the literature, especially for larger (multi-kilometer) craters. Besides existing generalized crater databases [e.g., *Barlow*, 1988; *Stepinski et al*., 2009; *Salamunićcar et al.*, 2011], global mapping efforts have identified large craters and used smaller craters to deduce stratigraphic relationships and ages [e.g., *Scott and Tanaka*, 1986; *Tanaka*, 1986; *Greeley and Guest*, 1987; *Tanaka and Scott*, 1987; *Tanaka et al.*, 2012]. In addition to global studies, regional or type studies have been completed, such as mapping craters on the poles [e.g., *Banks et al.*, 2010], mapping fresh craters [e.g., *Boyce and Garbeil*, 2007], identifying craters formed in the last few years [e.g., *Byrne et al.*, 2009; *Daubar*, 2011] determining ages of major impact basins [*Nimmo and Tanaka*, 2005], and age-dating larger craters themselves [*Werner*, 2008]. What has not been previously shown is the global distribution of small, kilometer-scale impact craters, and this work is the first such study to address this issue.

2.1. Craters with Diameters Larger than 3 km

This database contains 79,723 craters with diameters $D \geq 3.0$ km. Only two basins are included – Prometheus near the Martian South Pole, and Ladon near eastern Valles Marineris due to their clearly defined, if partial, rims. Other well known basins (such as Argyre, Hellas, or Utopia) or quasi-circular depressions [*Frey*, 2008, and references therein] were not included because their rims are more ambiguous and have been studied in much greater detail by other researchers [*e.g.*, *Schultz et al.*, 1982; *Tanaka et al.*, 2012]. The next-largest crater included is an unnamed 512-km-diameter crater, and there are 300 others that are $D \geq 100$ km. Generally speaking, this database contains more craters larger than 100 km than other databases [*Barlow*, 1988; *Stepinski et al*., 2009; *Salamunićcar et al.*, 2011], but not as many as found by *Frey* [2008]. Craters at smaller diameters ($3 \leq D < 100$ km) are also approximately 10% more numerous than found in those databases [see *Robbins and Hynek*, 2012, this volume, Section 7], which is likely due to use of the latest imagery in combination with global topography to identify craters.

2.2. Small Craters (1-3 km)

The small, $1 \le D < 3$ km crater distribution on Mars is illustrated in Fig. 1. The distribution of small craters can be used as a proxy for estimating relative regional ages where more craters indicate an older surface and fewer craters indicate a younger surface, though this is significantly complicated by local and regional resurfacing [*Grant and Schultz*, 1993; *Tanaka*, 2000]. Readily visible as young surfaces due to their relative paucity of craters are the major basis Argyre and Hellas, the Olympus Mons volcano and three Tharsis Montes, Elysium Basin, Valles Marineris, and both polar caps. More locally, there is clear contamination from secondary crater fields closely surrounding individual large primary craters such as Lomonosov (65.3°N, -9.3°E) and Oudemans (-9.8°N, -91.8°E) (see *Robbins and Hynek* [2011b] for a discussion of these fields). In addition, arcs of craters through Isidis are visible, likely emanating from Lyot crater (50.8°N, 29.3°E), and these have been interpreted as secondary crater clusters from that large impact [*Robbins and Hynek*, 2011a].

2.3. Fresh Craters

Crater preservation/degradation/modification states were classified on a four-point scale. This was determined by examining each crater rim for sharpness and relief (1-4 pts), ejecta preservation (1-3 pts), floor infilling (1-4 pts), and relative depth/Diameter ratio (1-4 pts, determined based on latitude region; see Section 5). Points were added and then scaled to a final 1-4 class where 1 was the most modified and 4 was a pristine or nearly pristine crater as viewed with 100 m/pix scale images. (See *Robbins and Hynek* [2012], this volume, for more detailed discussion of this system.)

On an airless and geologically dead body, the distribution of fresh craters is nominally uniform over the surface since it should be of a uniform older age, though recent modeling work suggests a small latitude dependence based upon orbital mechanics may be present [*Le Feuvre and Wieczorek*, 2008]. On a body with an atmosphere and more recent geologic activity, such as Mars, the fresh crater distribution is instead a likely indicator of volcanic and aeolian

123 erosion/modification efficiency across the planet [e.g., *Greeley et al.*, 1992; *Grant and Schultz*,
124 1993] and periglacial processes on small craters near the poles. Fig. 2 shows the global
125 distribution of $D \geq 5$ km fresh craters, and Fig. 3 shows the percentage of fresh $5 \leq D \leq 50$ km
126 craters relative to all craters in that range. As a basic result, these show that erosion across the
127 planet is far from uniform. Fresh craters are concentrated towards the equatorial regions and in
128 specific mid- to high-northern latitudes (between ~100-300°E). They are also more frequently
129 found on younger terrain, as expected: Spatially, there are 14.5 fresh craters $D \geq 5$ km per 10^6
130 km^2 of Noachian terrain, 24.8 for Hesperian, and 17.3 for Amazonian. More degraded craters
131 are found at the mid- to high-southern latitudes, agreeing well with the "softened" terrain of Mars
132 that has been discussed previously in the literature [*e.g.*, *Jankowski and Squyres*, 1992].
133 The data show the greatest fractional concentrations of fresh craters (Fig. 3) are centered
134 around the major volcanic provinces (Tharsis, Elysium, and Syrtis Major) and the three basins
135 Chryse, Isidis, and Utopia. A smaller concentration is also located between the two volcanoes
136 Tyrrhena and Hadriaca Paterae. One can conclude from this that fresh craters are at least $2\times$
137 more populous on younger terrain, especially volcanic, than most other surfaces. Volcanic
138 terrain in general is stronger and so can better preserve these features. There is also a general
139 abundance above the average in the mid- to high-northern latitudes that likely reflects their
140 relative youth.

141 3. Crater Morphologies Across Mars

142 Crater interior and ejecta morphologies are included in this release for craters $D \geq 3$ km.
143 The interior morphologic classifications include basic type (simple or complex) if it could be
144 determined and notes of central peaks, central pits, and summit pits. Morphology descriptors of
145 wall features such as terraces and secondary floor features such as faulting, channels, dunes, and
146 other floor deposits are also noted. Ejecta morphologies and morphometries are detailed for
147 Martian cohesive layered ejecta blankets. The general distributions and properties of crater

morphologies are described in this section and compared with previous works.

3.1. Distribution of Central Peaks, Pits, and Summit Pits

A classic feature of a fresh complex crater is a central peak, produced by rebound during the crater formation process [*e.g.*, *Wood*, 1973, *Roddy*, 1976]. Central peak craters number 3072 in this database. They represent a global average of ~6.3% of all craters $D \geq 15$ km, yet they comprise a disproportionate number of fresh craters (>90% of fresh craters $D \geq 15$ km contain central peaks). This likely indicates that many craters classified as "CpxFF" (complex, flat-floored) or "CpxUnc" (complex, unclassifiable) were originally central-peak craters but the peak has since been buried or eroded and is now not detectable. This interpretation is supported by Fig. 4 (the fraction of craters $5 \leq D \leq 50$ km with central peaks) which clearly shows that central peak craters are generally present in a relatively even fraction throughout most of the planet.

The data do show a noticeable deficit in a band of the southern highlands arcing from Argyre basin up to the equator at the prime meridian and back down through Hellas that does not correlate well with fresh craters (Fig. 3). The fraction of central peaks is mildly enhanced in Arabia Terra and in the southern highlands south of ~60°S and between East longitudes ~-90° to ~+90°. These suggest that this area has experienced enhanced erosion, in agreement with numerous previous studies that have indicated this area has experienced massive erosion, with suggested sources as polar wander [*Schultz and Lutz*, 1988; *Tanaka*, 2000] or running water [*Hynek et al*., 2002].

A feature of some central peak craters on Mars is a pit in the middle of the peak to which a classification of "summit pit" is given [*Barlow and Bradley*, 1990]; these are also observed on the Moon and Mercury. Martian craters as well as those on Jupiter's moons Ganymede and Europa also sometimes display central pits; these pits are occasionally observed in simple craters. Explanations for the genesis of these pits on crater floors or peaks are varied and include (1) vaporization of volatiles within the target during crater formation which releases gas near the center of the forming cavity [*Wood et al*., 1978; *Senft and Stewart*, 2008], (2) collapse of a

central peak [*Passey and Shoemaker*, 1982], (3) excavation into layered target materials [*Greeley et al*., 1982], (4) a melt-drainage model whereby liquid produced near to and during the impact forms a transient lake in the crater center that subsequently drains into the subsurface, leaving behind a central pit [*Croft*, 1981; *Bray et al*., 2006; *Alzate and Barlow*, 2011], and/or (5) displacements related to the compression stage of crater formation [*Schultz*, 1988]. The percentages of craters with summit pits (672 craters) are shown in Fig. 5, and the percentages with central pits (1841 craters) are shown in Fig. 6.

It is difficult to draw many conclusions from the distribution of summit pit craters because of the "small" numbers involved – despite this being the largest study ever done – though they do generally agree with findings by *Barlow* [2011]: They are prevalent in Arabia Terra, southwest of Tharsis, and southwest of Elysium. They appear to correlate well with the distribution of central peaks. This would not be surprising if their genesis is of the collapse mechanism suggested by *Passey and Shoemaker* [1982]. However, there is a noticeable enhancement in the distribution north of Tharsis, and this is not observed in the central peak distribution. There is likely a cryosphere near the surface at higher northern latitudes [*Boynton et al*., 2002] that could indicate a volatile-dependent origin. However, the significance of this is questionable: In each bin at that latitude (60-70°N), the number of craters with summit pits is 1.

Central pit craters (Fig. 6) are found to be enhanced relative to the global average around all volcanic centers, in general agreement with findings by *Barlow* [2011]: Tharsis, Elysium Syrtis Major, the Tyrrhena-Hadriaca corridor, and southwest of Hellas around Pityusa, Amphitrites, Peneus, and Malea Paterae. While these correlate with the fresh crater population, this is likely because the fresh craters correlate well with the volcanic terrain. There is also an enhancement near the prime meridian and in the range about 0-30°S latitude that is not related to volcanic landforms.

Subsurface ice near the equatorial Martian latitudes is not stable unless obliquities are >27°, and it is not stable in the Elysium region until obliquities are >30° [*Mellon and Jakosky*, 1995]; if ice is present today near the equator, it is likely buried far below the surface [*Clifford*,

1993; *Boynton et al*., 2002]. If the evacuation into subsurface liquid water reservoirs were the formation mechanism of central pits on Mars, though, one would expect significant concentration of central pit craters near the poles; this is not observed. Even though Mars' present-day obliquity is probably low compared with the long-term average, central pits are broadly concentrated in equatorial regions. This would require that the vast majority of these craters – which are a non-trivial fraction of the overall craters - formed when obliquities were >60°, which is fairly unlikely [*Laskar et al*., 2004]. Similarly, central pit craters are generally among the fresh crater population (92% were a preservation state of 3 or 4), and they are missing in the high southern latitudes where central peaks were prevalent. Thus, they are likely not a collapse from a central peak. Of the five proposed mechanisms, none have predictions of the distribution of central pits that matches that in this database, though it is not possible to draw a prediction from the proposal in *Schultz* [1988]. The now-favored melt-drainage model in the literature [e.g., *Alzate and Barlow*, 2011] appears to be less likely given the distribution, though it cannot be ruled out.

However, one must keep in mind that while these data do not support any of the four proposed mechanisms, it is entirely possible that the distribution is an artifact of preservation across the planet. With 92% of central pit craters being fairly fresh, and a topographic depression being the first to fill with any material, there is likely a significant observational bias. If there is any target- or geologic-related bias in their formation, at best it can be concluded that these are still an enigmatic feature with a formation that cannot be gleaned from a simple present-day global distribution approach.

3.2. Ejecta Morphologies

Crater ejecta usually indicates youth, and on the Moon it is useful for geologic mapping and age relationships. On the Moon, craters display a radial ejecta morphology where the material has been ballistically emplaced during the excavation phase of crater formation as individual particles ejected during impacts. When probes returned the first images of Mars, a

wholly new class of ejecta was observed. The terminology has varied significantly over the years [see discussion in *Robbins and Hynek*, 2012, this volume], but the term "layered ejecta" is now part of the standardized nomenclature [*Barlow et al*., 2000]. This database contains morphologic indications for ejecta and morphometric data for the layered type that are explored in brief in this section for craters $D \geq 3$ km.

3.2.1. Radial Ejecta

Of the 79,723 craters $D \geq 3$ km in this database, radial ejecta is the sole ejecta type in 24,897 craters (31.2%). A crater was considered to have radial ejecta if there appeared to be radial patterns radial to the rim; this could include eroded ejecta where all that remains are remnant patterns [*Schultz*, 1992]. The spatial density on each terrain type per 10^6 km^2 is: 161 Noachian, 54 Hesperian, and 23 Amazonian. It is clear from this that radial ejecta patterns on Mars can still be visible around ancient craters, otherwise the distribution should be even if one assumes craters form uniformly across the different terrain types. In fact, the relative densities are more disparate than those from the fresh crater population, as one would expect if this were the case.

3.2.2. Layered Ejecta

When Martian layered ejecta craters were first examined, it was thought they were part of a type evolution that started with multi-layered craters that erode to single-layer ejecta craters that finally erode to pedestal craters [*McCauley*, 1973]. *Woronow and Mutch* [1980] and *Mutch and Woronow* [1980] were among the first to quantitatively examine the geometric properties of the ejecta of each and determine they are not evolutionarily related. Over the years, two hypotheses emerged and remained for a formation process of the layered ejecta. One holds that they are formed when an impactor hits a volatile-rich sub-surface, the impact energy melts or vaporizes the volatiles, and the ejecta acts like a fluid as a result [e.g., *Carr et al.*, 1977]. The other states that they form when the severity of the impact causes atmospheric vortexes and

winds [e.g., *Schultz and Gault*, 1979; *Schultz*, 1992]. It is possible a combination of both models is at work on Mars [e.g., *Barlow*, 2005; *Komatsu et al*., 2007].

Over the years, these forms of ejecta have only been observed on Venus, Mars, Ganymede, and Europa [e.g., *Barlow et al*., 2000; *Boyce et al.*, 2010]. The lack of atmosphere on Ganymede and Europa indicates that an atmosphere and hence the atmospheric vortex model may not be required for the formation of these kinds of ejecta, but the intense surface heat on Venus suggests that volatiles within the impact medium may also not be necessary in some formation situations. Determining the morphometric characteristics of each should help constrain these and discriminate between the two in different cases. Motivationally, if it can be shown that morphometric analysis required volatiles for the ejecta to form, then high concentrations of these crater types could indicate where subsurface water may be for future human exploration. To this end, an introduction to the distributions and characteristics is presented here, and future work will focus on combining these with mineralogic, thermal inertia, and crater age dating of the ejecta blankets themselves to distinguish between the models.

Of the 79,723 craters $D \geq 3$ km in this database, a total of 18,841 are surrounded by layered ejecta blankets: 14,679 are single-layered (SLE), 3333 are double (DLE), and 829 are multiple (three or more) (MLE). (See *Robbins and Hynek* [2012], this volume, for a detailed description of all ejecta morphologic and morphometric properties in the database.) The Barlow Database [*Barlow*, 1988] for craters $D \geq 5$ km contains 3221, a factor of $\sim 4\times$ fewer over the same diameter range for this database. There is a size dependence observed on the number of layers. The largest SLE crater is a 111-km-diameter crater, the largest DLE is 78 km, and largest MLE is 83 km. These could be considered outliers, though, and insignificant in determining the onset of these features because all types start to increase dramatically on a size-frequency diagram at $D \sim 30-40$ km; they are statistically identical in frequency for $D \gtrsim 20$ km. For MLE, the peak in frequency is sharp at $D = 17$ km; it is rarer for a crater to display MLE blankets at smaller diameters. The peak for DLE is at 12 km, and the peak for SLE craters is at approximately 5.3 km. Both DLE and SLE craters have fairly constant numbers for diameters

~3-16 km and ~3-7 km, respectively, though these form a decreasing fraction of the overall craters at smaller diameters.

These craters are not distributed uniformly across the planet, a feature that has been known for many years (and characterized, for example, in *Barlow* [1988]). When examining the latitude-dependence, Fig. 7 clearly shows these craters are more numerous in the northern hemisphere and especially at high northern latitudes 50°-80° N. The enhancement around 10°N is likely due to volcanic terrain abundance at this latitude, discussed below. *Barlow and Perez* [2003] and *Barlow* [2005] found a relatively even distribution across the planet with a marked spike ~65-80° N. Another feature of the Barlow Database that this catalog reproduces well is the significant increase of DLE craters ~40-75°N (though *Barlow and Perez* [2003] found a tighter latitude range).

Expanding this distribution in longitude, Fig. 8 shows all SLE, DLE, and MLE craters as a fraction of all craters within a $5° \times 5°$ bin, similar to analyses in *Barlow and Perez* [2003] from Viking data. Clearly visible are several trends. First, SLE craters dominate all volcanic terrains (that have a significant number of craters on them). They also dominate in the high northern latitudes. DLE craters are similar though they clearly dominate at higher northern latitudes as indicated in Fig. 7. In general, there was no longitude dependence upon the distribution of DLE craters, though there was a slight increase in the eastern Tharsis and lower Valles Marineris region. It is difficult to draw conclusions from the MLE distribution due to small numbers (even at coarser binning, global trends are not apparent). The most that can be confidently stated is that the MLE distribution does not disagree with the SLE distribution, and there is an enhancement around Elysium. These all agree with the general conclusions from *Barlow and Perez* [2003] with the main anomaly being the concentration of SLE craters to the southwest of Valles Marineris. This could be an artifact of the way the data are presented: In Fig. 7, LE types are shown as a fraction of all craters, but in *Barlow and Perez* [2003], the data are discussed and displayed as a fraction of craters with ejecta.

A morphometric characteristic examined is ejecta mobility, the extent to which the ejecta travels relative to the crater radius. This database uses the average extent, following *Barlow* [2005]. It reproduces those findings well, though the average ejecta mobility is a little less and the maximum extents were a little more in this work (see Table 1). An additional feature identified in early work [*Mouginis-Mark*, 1979] is a latitude dependence with ejecta mobility where, near the poles, the average is up to 2.0 versus the equatorial average of 1.4. This catalog's data show a similar trend with the transition happening at ~±30-40°. Ranges poleward of ±40° were examined separately from an equatorial region ±30°, and values are reported in Table 1. Polar crater layered ejecta is found to travel farther than equatorial, while that in the northern hemisphere travels farther than in the south.

4. Crater Shapes

Basic crater shapes have been measured for decades [e.g., *Pike*, 1976], and this database provides the ability to verify and update these morphometric values on Mars. Only fresh craters $D \geq 5$ km of preservation class 4 were used for this analysis (1964 simple and 1413 complex). This section addresses crater rims and surface-to-floor scaling, separate from scaling of crater depth (rim-floor) as a function of diameter which is described in Section 5. Both of these rely upon accurate rim height measurements, a value that is in question given the relatively coarse nature of Mars Orbiter Laser Altimeter (MOLA) [*Zuber et al.*, 1992; *Smith et al.*, 2001] gridded data. The fidelity of measurements in this database was addressed in detail in *Robbins and Hynek* [2012], this volume, which found them to be reliable for these purposes: To within the uncertainty quoted in the database in rim heights, it was found that the measurements from gridded data were accurate when compared with the MOLA point data. In this database, extreme values were ignored: Rim, surrounding surface, and floor elevations were measured as the average of N topographic data points for each. Throughout this section, comparison data are from *Pike* [1976, 1977], *Wood and Andersson* [1978], and *Hale and Head* [1979] as summarized

by *Melosh* [1989].

The first feature often addressed is rim height above the surrounding surface. At a basic level, this scales with crater diameter, and generalized results based on lunar data show that rim height is ~4% of the crater diameter. However, examination of the Martian craters in this database shows a well-defined Gaussian distribution of this relationship for simple craters 1.9±0.7% and 1.4±0.6% for complex craters. This rim height is $>2\times$ smaller than what is typically reported. A possible explanation is that this database uses the average elevation around the crater rim instead of the highest point, but that is unlikely to be able to account for this large of a difference. Similarly, *Melosh* [1989] quotes from the above-mentioned aggregated sources that the surface-to-floor depth of simple craters is ~20% the crater diameter, but the simple craters in this database have a relationship of 8.9±1.9%. This is again $>2\times$ smaller than what is typically reported. Complex craters are shallower with a surface-to-floor depth 6.2±1.9% the crater diameter.

When looking at a diameter-dependence for rim height, apparently fresh craters were examined in the method detailed below for depth/Diameter relationships. For these simple craters, a power law $h = 0.011D^{1.300}$ was fit, and a relationship of $h = 0.025D^{0.820}$ was found for complex craters (where h is rim height and D is crater diameter). In contrast, in ~6000 craters examined, *Garvin et al*. [2003] found $h = 0.04D^{0.31}$ for simple craters (significantly different) but $h = 0.02D^{0.84}$ for complex (statistically identical). Better topographic data for smaller-diameter craters should help determine which - if either - is accurate.

Another way to examine scaling is to measure rim height relative to the overall rim-to-floor crater depth. This is found to follow a Gaussian with a mean 16±6% for simple craters and 18±6% for complex craters. The similar values indicate that the uplift and overturn that results in rim formation scales well through these two crater morphologies.

5. Global depth/Diameter Relationships

355 The ratio of a crater's depth to its diameter is one of its most fundamental properties, but
356 it is one that was not directly measurable for extraterrestrial craters until the last two decades.
357 Prior, crater depths were estimated through photoclinometry and shadow lengths, processes that
358 rely on knowing sun angles and the former assuming a uniform surface albedo [e.g., *Chapman*
359 *and Jones*, 1977; *Pike*, 1976, 1977, 1980, 1988; *Davis and Soderblom*, 1984]. With the inclusion
360 of the MOLA instrument on *Mars Orbiter*, global laser altimetry data has allowed for the
361 uniform measure of crater topographic properties provided in this database. These were
362 measured from the MOLA gridded data (MEGDR) as described in *Robbins and Hynek* [2012],
363 this volume. Briefly, crater rims and floors were identified in MEGDR data and the average
364 elevation of points along the rim and deepest sections of the floor were used to compute the rim-
365 to-floor depth. This was found to be accurate when compared with the MOLA point data
366 (PEDR), as limited random sampling performed in *Robbins and Hynek* [2012], this volume,
367 suggests the recorded values are accurate to within the uncertainties that were also recorded.
368 Future work comparing these data with the *Mars Express*'s High-Resolution Stereo Camera
369 (HRSC, *Neukum and Jaumann* [2004]) should clarify this, but at present the MOLA data are still
370 used. Throughout this work, the "rim-to-floor" depths were used unless otherwise stated.
371 Previous work by *Garvin et al.* [2003] estimated a $d = 0.21D^{0.81}$ relationship for simple
372 craters $D \leq 6$ km, and $d = 0.36D^{0.49}$ for complex craters $D > 6$ km. *Boyce and Garbeil* [2007]
373 find a similar curve of $d = 0.315D^{0.52}$ for complex craters $D \geq 7$ km. While hesitant to quote a
374 global average for reasons discussed below, this database yields a simple crater relationship of
375 $d = 0.179D^{1.012}$ and a complex one of $d = 0.286D^{0.582}$; these are comparable to previous works,
376 though there is some variation as one may anticipate, as discussed below.

377 5.1. Regional depth/Diameter Relationships

378 Across the surface of a planetary body, one might expect the ratio of a crater's depth to
379 diameter to be reasonably constant; on Mars, however, a fresh-looking crater's observed depth
380 can vary significantly depending upon where it formed, as shown throughout this section. This

affects any "global" depth/Diameter ratio (d/D) one may quote, though this has been done throughout the literature for decades [e.g., *Pike*, 1980; *Garvin et al*., 2000, 2003; *Boyce and Garbeil*, 2007; *Stepinski et al*., 2009]. To illustrate this, craters were separated by simple and complex morphologies and then into different diameter ranges. Diameter ranges within each morphology were done because there is no set ratio for the d/D value for fresh simple or complex craters – even though it is often quoted as 1:5 and 1:10-100, respectively [*Pike*, 1977; *Melosh*, 1989].

All craters were divided into six diameter ranges that each encompassed roughly a factor of $2\times$ in size. Smaller ranges had small-numbers problems that limited the overall utility, while larger ranges muted the differences and hence analysis that could be done. Simple craters were separated into two ranges – 3-5 km (N=20,309) and 5-7 km (N=4366). Complex craters were separated into four: 7-15 km (N=14,449), 15-30 km (N=9097), 30-50 km (N=3260), and 50-100 km (N=1236). Craters were then binned into $10°\times10°$ latitude/longitude bins and the mean d/D value was calculated; bins with <5 craters were removed. These are shown in Fig. 9. A similar analysis was done for fresh craters only (preservation states 3 and 4), illustrated in Fig. 10, in $30°\times30°$ bins. The results were comparable given the limitations, as discussed below.

Readily apparent from Fig. 9 is significant global variation. To first-order, craters $D \lesssim 20$ km poleward of $\sim\pm40°$ latitude are significantly shallower than their counterparts closer to the equator by as much as a factor of $2-3\times$. Second-order effects are that craters near the major volcanic complexes - Tharsis and Elysium - are deeper than the general average, and craters within the Isidis, Utopia, and northern Chryse / southern Acidalia impact basins are the deepest on the planet, on average. Similar results were observed by *Boyce et al*. [2006], except they did not identify this effect in northern Chryse (this was not in their study area). In the equatorial range, the shallowest craters are within Arabia Terra, unique from the southern highlands. The patterns noted here disappear at larger crater diameters, or at least as far as can be determined from the smaller numbers. The last remnants of the pattern are in the 15-30 km range, showing deeper craters around Tharsis and Elysium and shallower craters towards the

north pole, but not the south. $D > 30$ km craters do not show this.

Analysis of the relatively fresh crater population (preservation states 3 and 4) shown in Fig. 10 support the majority of these observations: Craters are shallower near the equator and deeper near the poles, and this effect persists up to the $D \leq 30$ km range. The more localized findings of deeper craters in the northern hemisphere basins is not found, though this is likely because of small number statistics; finer binning in the $3 \leq D < 7$ km simple crater range removes bins over those regions due to small numbers, so the effects are averaged out at the coarser binning shown. Deeper craters at small diameters are observed over the Tharsis region, though. The shallower craters observed in Arabia Terra are not found at smaller diameters but are somewhat visible between 7 and 30 km, though the difference is slight. This overall agreement between Figs. 9 and 10 support the interpretation that Fig. 9 is generally indicative of the fresh crater population and the interpretations that follow.

The equatorial/polar dichotomy disappearing for $D > 30$ km craters can be interpreted as larger craters excavating to a more uniform basal layer across the planet, and subsequent modification occurs more uniformly and is less controlled by regional upper crust strength. The pattern at smaller diameters of shallower craters towards the poles is likely explained by a near-surface cryosphere [*Boynton et al.*, 2002] that is weaker and cannot support a deep crater, relaxing to a shallower depth during the crater modification stage and subsequent geologic time. This implies that the crust overlying the major impact basins Chryse, Isidis, and Utopia, is stronger than the average Martian surface today, supporting the deeper crater cavities. Expanding upon the argument from *Boyce et al*. [2006], this shows that the local crust is stronger by at least a factor of $2\times$ than most other surfaces on Mars. Mineralogical mapping in future work may help characterize the rock, as there are suggestions of regional olivine-rich volcanic units in southern Isidis that may play a role in this [*Hamilton et al*., 2003; *Hoefen et al*., 2003]. Alternatively, the similarity with deeper craters on volcanic terrain and the gravitational load in the regions suggest these basins may be buried by volcanic material, and that could be stronger than the average Martian crust to ~1 km depths [e.g., *Searls and Phillips*, 2007]. A separate

435 hypothesis is that the terrain may be particularly fine-grained in some areas of these basins, and
436 work suggests [e.g., *Soderblom et al*., 1973, 1974; *Schultz and Lutz*, 1988] that fine-grained fill
437 materials can produce anomalously deeper craters and this material is found in at least some of
438 these regions.

439 5.2. The Depth-Diameter Relationship for Mars

440 5.2.1. Variation with Latitude and Terrain Type

441 As is readily apparent from Fig. 9, except for craters $D \gtrsim 30$ km there is no uniform,
442 global depth/Diameter ratio even for a small diameter range that can be quoted for the planet
443 because of a significant shallowing near the poles. This must be taken into account when
444 considering a relationship "for Mars" and when using it to determine different properties at an
445 automated level, such as its role in classifying crater preservation state. Besides being important
446 from a physical standpoint and understanding the near-surface crust, it is necessary to have an *a*
447 *priori* estimate for how deep a crater likely was when it formed for purposes of estimating
448 erosion and infilling. For example, if one were to use a global estimate for a D = 5 km simple
449 crater (d = 0.8 km) and found it to be filled with lava with 0.2 km deep cavity remaining, then
450 one would assume 0.6 km of burial. But, if this crater was poleward of ~40°, the actual d/D
451 relationship yields a fresh-looking crater depth of $d \approx 0.3$ km, so there is only 0.1 km of infill.
452 In the sub-sections following 5.2.2, craters were separated into seven different regions:
453 First, a global average was done as has been worked on for several decades for comparison
454 purposes. Next, two latitude ranges were analyzed based upon Fig. 9 and Section 5.2.2 –
455 poleward of ±40° and equatorward of ±40°. Finally, four terrain types were analyzed based on
456 geologic maps by *Scott and Tanaka* [1986], *Greeley and Guest* [1987], and *Tanaka and Scott*
457 [1987].

458 5.2.2. Bimodal Nature

459 *Stepinski et al.* [2009] clearly showed d/D are bimodal for craters equatorward of ~±40°,

460 the deep craters being "severely depleted southward of ~38°S." Their work was among the first
461 to study this in a broad, systematic way, though they used a sub-set of 2444 craters to do so.
462 Previous research by *Mouginis-Mark and Hayashi* [1993] used 109 fresh craters 20-40°S and
463 found a general shallowing trend farther south, but their lack of large numbers of craters limited
464 the spatial analysis and robustness of their work. *Mouginis-Mark and Hayashi* [1993] attributed
465 this to a cryosphere, and *Stepinski et al*. [2009] identified this as a possible contributor, as well.
466 *Stepinski et al*. [2009] also raise the possibility of surficial mantling deposits as suggested by
467 *Soderblom et al.* [1973, 1974]. *Kreslavsky and Head* [2003] propose summertime melting of
468 ground ice at ±40-50° latitude which could also be a cause. *Boyce and Garbeil* [2007] used a
469 test population of 6047 craters throughout the planet and concluded with a different
470 interpretation: They suggest there is a gap in crater ages separated by the Late Noachian / Early
471 Hesperian boundary that was the result of "abrupt onset and cessation of an episode of terrain
472 degradation" as suggested by *Craddock and Maxwell* [1993]. This would reflect a very rapid 10
473 μm/yr erosion/infill rate (current estimates are ~1-10 nm/yr [*Golombeck et al.*, 2006]). They
474 suggest the contrast with higher latitudes indicate these erosion processes were not active there
475 or other processes erased their effects.

476 Similar results are found in this database, as illustrated in Fig. 11. Simple craters tended
477 to have slightly deeper *d*/*D*, as would be expected from Section 5.1; so, they are not plotted
478 separately. In Fig. 11, two different datasets are shown – the overall results for all craters as
479 small red dots and craters with a preservation state of 3 and 4 as larger blue dots. This work
480 finds results similar to *Boyce and Garbeil* [2007] and *Stepinski et al.* [2009], but from a larger
481 database, more detail can be gleaned.

482 First, the same pattern of a gradual *d*/*D* decrease in the deepest craters occurs over the
483 ~10° range of ±30-40° latitude. However, the north and south hemispheres vary in the
484 magnitude of the difference. In the south, which is where previous studies looked (likely due to
485 the larger crater population in that hemisphere), the *d*/*D* changes from a relatively tight cluster
486 around ~0.08-0.14 and decreases to ~0.04 with outliers that go up to ~0.10. In the northern

hemisphere, there is significantly more spread with *d*/*D* ranging from ~0.08 up to ~0.20. In the higher northern latitudes, there is a shift where a large number of craters are concentrated at shallow ~0.02 ratios but with a nontrivial number of craters as deep as ~0.05-0.10 at high northern latitudes. Most of this is reflected well in the "all craters" population in Fig. 11.

Another observation is that the pattern is mirrored in the fresh craters, but this begs the question of what is considered "fresh" at ±~60° latitudes. The relatively large fraction (up to ~1/3) of craters in higher northern latitudes that were classified as "fresh" [see *Robbins and Hynek*, 2012, this volume] implies that many of these may not be as pristine as they appear. Numerous researchers [*e.g.*, *Schultz and Lutz*, 1988; *Tanaka*, 2000, *Head et al.*, 2003] have discussed the true polar wander of Mars over 10^5-10^6-year timescales which are much shorter than the formation time of these craters [*Ivanov*, 2001]. While they were interpreted as "fresh" given the morphologic and morphometric criteria discussed in the companion paper, they have likely experienced some amount of infilling.

An interpretation is the northern / southern hemisphere discrepancy can be partially explained by the presence of large impact basins and volcanic complexes in the northern hemisphere that contain the deepest craters on the planet (see Section 5.1). However, this is not adequate for the higher northern latitude discrepancy. A possible explanation is that the crust in the southern hemisphere may be more cohesive and stronger, allowing it to support deeper crater cavities, though this seems to run contrary to the "softened" terrain found in higher southern latitudes [*e.g.*, *Jankowski and Squyres*, 1992]. In the north, the ice table may be both thicker and closer to the surface – indeed, *Phoenix* at 68.22°N found ice just a few centimeters from the surface [*Smith et al*., 2009]. The enhanced relaxation cannot support deep craters, so even otherwise morphologically fresh craters are still comparatively shallow. Another possible contributing factor could be there is more diverse terrain in the higher southern latitudes than in the north. In the north, the northern part of Tharsis and Utopia are present, but otherwise the terrain is predominantly the low northern plains and polar cap. The high southern latitudes contain major volcanoes, the southern half of the comparatively fresh Hellas and Argyre basins,

514 southern highland terrain, and the residual polar cap. While these are offered as likely
515 contributing factors, this should be an area of future investigation.

516 5.2.3. Deepest Craters Method

517 Arguably, measuring the deepest, freshest craters is likely to produce the best estimate of
518 the original, pristine, crater depth-to-diameter ratio. This method has been utilized in the past
519 several times, notably by *Garvin et al.* [2003] and *Boyce and Garbeil* [2007]. The former used
520 the deepest 25% of their simple craters from which they estimated a $d = 0.21D^{0.81}$ relationship
521 from 469 craters for $D \leq 6$ km, and $d = 0.36D^{0.49}$ for complex craters $D > 6$ km. The latter
522 examined craters $12 \leq D \leq 49$ km and found a relationship of $d = 0.315D^{0.52}$.

523 The methodology of *Boyce and Garbeil* [2007] is what was used here: They separated
524 craters into diameter size bins and iteratively used the single deepest, average of the two deepest,
525 average of the three deepest, etc. craters in each bin through which to fit a power law. They
526 found the slope of the power law was a constant 0.52±0.004 despite increasing the number of
527 craters, while the amplitude of the power law fit changed from 0.363 to 0.356 to 0.333,
528 decreasing with increasing numbers of craters. This was expected and helped to confirm they
529 were sampling the results of the underlying physical process rather than secondary effects, and it
530 produced a more robust result. The value quoted above is for the five deepest craters.

531 Repeating their example, craters from this database were binned in multiplicative $2^{1/8}D$
532 bins. The deepest two craters were averaged together and a power law fit, then the deepest 3, 4,
533 5, 10, 15, 20, and 25 per bin. For complex craters $6 < D < 90$ km, the exponent reached a
534 constant level for ≥3 craters per bin with a mean 0.582±0.008. While this is slightly greater than
535 their value, it is still fairly close and can be explained because of the use of a larger dataset and
536 diameter range. Also similar to their results, the amplitude started large at 0.360 and proceeded
537 to decrease linearly when including 4 or more craters. While a smaller amplitude is reported
538 here than in *Boyce and Garbeil* [2007], this can be explained in that their definition of crater
539 depth was average rim height to the deepest pixel on the floor; the definition used in this

database was average rim height and the average of at least 3 floor pixels.

The analysis for simple craters was not as straight-forward. The exponent on the fit varied significantly until at least four craters were included, at which point the mean was 1.012 ± 0.020. This is steeper than *Garvin et al.* [2003], but the robustness of this exponent in other analyses in this work indicates it is likely not anomalous. The amplitude of the fit decreased dramatically from a maximum of 0.271 to an average of 0.179 ± 0.001 for the 10-25 deepest crater fits.

Based on this work, the averages are what will be quoted as the "final" values for the global depth/Diameter relationship on Mars for these craters and are reported in Table 2. The amplitude from the 4 deepest craters fit for complex craters is used because that was the onset of an observed linear decline. When exploring this further, the craters were separated into regions – northern plains, southern highlands, polar, and volcanic – and separated by latitude – equatorward of ±40°, and poleward of ±40°. The regressions were again run, and the results are in Table 2.

Both simple and complex craters poleward of ±40° latitude had no convergence upon a single value for either the exponent or amplitude of the fit for simple and for complex craters. This may be due to relatively small number statistics, but there were still several thousand craters being analyzed and this is an unsatisfying and unlikely reason. Since it is for $N = 10$ craters that a predictable pattern emerged, it is those values quoted in Table 2 and used in determining crater preservation state for this latitude range (see *Robbins and Hynek* [2012], this volume). A similar pattern was present for $N \geq 5$ craters for the complex craters, thus, it is the $N = 5$ regressions quoted in Table 2 and used to determine crater preservation state. Of interest, the complex slope is very similar to that for the globe, but the slope for simple craters is significantly shallower. This is likely due to two main reasons. First, as identified in *Boyce et al*. [2006] and discussed in Section 5.1, the very deepest and largest simple craters are in Chryse, Utopia, and Isidis, generally south of 40°N latitude; while these will be included in the global analysis, their absence here will decrease the amplitude of the largest few diameter bins and hence decrease the

567 exponent. Related, the second likely contributing factor is that the crustal strength is
568 significantly less, and the inability to support deeper cavities will likely scale with crater
569 diameter, also decreasing this exponent.

570 While the relationship poleward of ±40° was subject to significant differences, perhaps
571 unsurprisingly the relationship equatorward of ±40° was very similar. This is easily explained
572 by the deepest craters being in this region of the planet and so an algorithm designed to capture
573 the deepest ones would pick up on these in a global distribution. Overall, the results are in good
574 agreement with the global average and are within the quoted ranges.

575 Analysis by terrain type for the deepest craters method yielded higher amplitudes for the
576 complex crater *d*/*D* relationship for all three analyzable terrains (polar craters numbered too few
577 to be analyzed with this method). The difference was greatest in the northern plains where the
578 amplitude was fully 67% greater than the global function. However, the exponent was
579 significantly shallower, only 62% of that for the global relationship. This would indicate that
580 smaller craters start out deeper in the northern plains but then do not increase in depth as rapidly.
581 Similarly, the exponent on the simple crater function for the volcanic terrain and southern
582 highlands was shallower while the amplitude was just slightly higher, indicating a similar trend
583 to complex craters in the northern plains.

584 5.2.4. Fresh Craters Method

585 Recent work to define the *d*/*D* relationship for Mars [e.g., *Garvin et al.*, 2003; *Stewart*
586 *and Valiant*, 2006] has generally relied upon identifying and measuring the depth and diameter
587 values of morphologically fresh/pristine craters. The *Garvin et al.* [2003] results are described
588 above and agree generally well with the deepest crater method. *Stewart and Valiant* [2006]
589 limited their analysis to five regions on Mars and examined relatively few craters in each:
590 Acidalia Planitia ($N = 29$), Utopia Planitia ($N = 53$), Isidis Planitia ($N = 24$), Lunae Planum
591 ($N = 48$), and Solis Planum ($N = 33$). Utopia and Isidis were identified previously in this work,
592 *Boyce et al*. [2006], and *Stepinski et al*. [2009] as having deeper craters than the average terrain,

593 and they found larger d/D when just looking in those regions ($d = 0.404D^{0.41}$ for Utopia and
594 $d = 0.351D^{0.41}$ in Isidis). Acidalia is north of the Chryse impact basin and is around the region
595 identified above as also having deeper than average craters, and they identified a relatively deep
596 crater relationship there, as well, of $d = 0.384D^{0.38}$. Interestingly, the slopes in all of these
597 relationships are shallower than identified by the work from this crater database, indicating that
598 they found, by comparison, either smaller craters to be deeper or larger craters to be shallower.
599 Another possible explanation is that there may be relatively large uncertainties due to the
600 comparatively small number of craters in their study.

601 The analysis in this section mimics this approach and only uses craters that are classified
602 with a preservation state of "4" (fresh). This process is slightly incestuous because one of the
603 four parameters in crater preservation state is the crater depth relative to the established d/D
604 relationship. To minimize how recursive this process is, the deepest crater d/D was used to
605 define that part of crater preservation state such that this fresh crater method could be relatively
606 independent. Overall, 2704 craters $D \geq 5$ km were identified as "fresh" in this database (an
607 additional 3603 craters $3 \leq D < 5$ km were fresh, but they were not used in this analysis due to
608 larger uncertainties). Of those, 934 were classified as simple (831 were equatorial of ±40° and
609 103 poleward), and 1060 were complex (976 were equatorial of ±40° and 84 were poleward).

610 As an overall global average, the slope of the fresh simple and complex craters was
611 similar to the deepest crater method, varying at the few-percent level and likely within the noise.
612 The amplitude of the fit is expectedly smaller, though the difference is roughly a factor of $2\times$
613 for simple craters but ~15% for the complex craters. This is easily explained in that the fresh
614 craters method is sampling an ensemble of terrains (the whole planet) and that the deepest crater
615 method is simply picking the deepest ones which have been shown to be terrain-dependent. The
616 relative lack of a difference at the larger, complex crater diameters can be interpreted as these
617 craters are less dependent upon terrain type than smaller craters and therefore there are fewer
618 deepest craters that then get averaged out.

619 Regressions were again run for the sub-regions, and the results are shown in Table 2.

620 Overall, the separation by latitude range is similar to the trend found for the deepest craters,
621 though small numbers towards the poles ($N = 103$ for simple and $N = 84$ for complex) may
622 limit the robustness of the fits. Analysis of the polar terrain craters could not be done because
623 the numbers were too small. Overall, the terrain separation did not yield significantly different
624 results than the global analysis except in three values. First, the exponent in the simple crater fit
625 for the northern plains was substantially steeper than both the global average and equatorial
626 range. Second, the amplitude for the simple craters in volcanic terrain was twice that of the
627 global average and the latitude separations, indicating that simple craters start substantially
628 steeper in volcanic terrain, but the exponent was smaller, indicating that as they increase in
629 diameter, the depth does not grow correspondingly as large as for the global average.

630 5.2.5. Average Across Crater Depths and Preservation States

631 An additional method that may have dubious intrinsic physical meaning is that of taking
632 an overall average of depths of craters for a given diameter. This was done in *Stepinski et al.*
633 [2009] to define $d = 0.025D^{1.6}$ for simple craters D < 7 km, and $d = 0.22D^{0.47}$ for complex
634 craters $D \geq 7$ km based on a combined total of 3666 craters. Earlier, *Garvin et al.* [2003]
635 produced overall average results for simple craters $D \leq 6$ km of $d = 0.21D^{0.80}$ from 2263 craters.
636 This is only slightly different from their results for the deepest craters, and it is significantly
637 different from the *Stepinski et al*. [2009] function.

638 Fitting was done in the same manner as the previous sections, and results are reported in
639 Table 2. In this case, *all* craters were included in these numbers. Globally, the complex crater
640 function was similar in slope to the overall average, though it was slightly shallower, and the
641 amplitude was 37%. This indicates that as a whole, Mars' crater population has been
642 infilled/modified relatively evenly across diameter ranges, though there may be slightly more
643 infilling at larger sizes. This is interpreted as larger craters are generally older and so would be
644 more infilled on average than a broader age range at smaller diameters. The simple crater
645 population is significantly different, for it has an amplitude of 26% the deepest craters but an

exponent 27% greater. Borrowing from the above interpretation, this indicates that more small simple craters are significantly infilled than larger ones. While this may be the case, it could also be an artifact of the MOLA data used in this analysis as discussed in *Robbins and Hynek* [2012], this volume, and the beginning of this section. Further work examining each crater with MOLA shot data and/or comparison with higher resolution DTMs are necessary to resolve whether the latter issue is a significant factor. Both of these are significantly different from *Stepinski et al*.'s [2009] results.

Division of the craters along the ±40° latitude lines resulted in somewhat different results to those found in Section 5.2.3 with the deepest craters. Poleward of ±40°, the amplitude of the fits decreased by a factor of $\sim 3\times$, while the amplitude of the fits for craters equatorward of ±40° increased by a factor of $\sim 1.5\times$. The equatorial craters' exponents dropped by ~20% while the polar simple craters rose by 14% and complex by 58%. This was the steepest complex crater relationship found in this work except for the polar terrain separation. Interpretation of these results for amplitude is straight-forward and discussed above, for polar craters are shallower because of a weaker crust likely due to a cryosphere. The hypothesis discussed above that the anomalously large exponent for simple craters may be due to MOLA artifacts should be less significant near the poles because of higher point density due to the *Mars Global Surveyor* orbit; thus, these results should be *more* robust than their equatorial counterparts, but the slope is greater. If this is a real phenomenon, this would indicate the former interpretation for the global results is more likely, that smaller craters are more infilled than larger ones, which would seem to belie a normal sequence of events: larger craters preferentially form earlier in the history of a surface while many more smaller craters form later. If one can assume an even infilling/erosion rate, the d/D slope should remain fairly steady while the amplitude decreases. More work on this issue should be done to unravel this result.

The all-crater average when craters were separated by terrain yielded a few interesting results. First, the polar terrain craters were significantly shallower than the global average, but the power law exponents were significantly steeper by 43% and 107% for simple and complex

673 curves. This could be explained by the proposal in Section 5.1: Smaller craters ($3 \leq D < 7$ km)
674 will be effected by the terrain much more than larger craters. Thus, the polar terrain will cause a
675 significantly shallower crater, but as craters get larger the terrain dominance lessens and normal
676 scaling dominates. An alternative explanation [*P. Schultz*, pers. comm.] is that smaller craters
677 may be more efficient at trapping deposits of ice and other material from a moving ice cap,
678 whereas larger craters could be more easily exhumed due to their boundary conditions.
679 Otherwise anomalous were the craters on volcanic terrain with amplitudes a factor of $2\times$
680 greater than the global average. However, this can be fairly easily explained by fresh craters
681 dominating Martian volcanic terrain (64% are preservation states 3 or 4) and so more modified,
682 shallow craters do not lower the average.

683 5.3. Synthesis of the depth/Diameter Relationship
684 Crater depth/Diameter relationships are an important tool to understanding how craters
685 form and then how craters differ from what is expected. Investigation into this relationship was
686 done in three main ways – deepest craters, fresh craters, and all craters – and for the entire globe,
687 different latitude bands, and specific terrain types. Overall, the results are reasonably consistent
688 with most previous work in this area [e.g., *Garvin et al.*, 2000, 2003; *Stewart and Valiant*, 2006;
689 *Boyce and Garbeil*, 2007] though varied from the automated analysis of *Stepinski et al*. [2009].
690 Within the nineteen different method-region combinations for both simple and complex
691 craters, the results were generally self-consistent. Variations were expected due to the particular
692 analysis conducted. For example, the deepest craters method consistently yielded the deepest
693 d/D relationship while the all-crater averages were always the shallowest. The exponent slopes
694 were also generally consistent among each other, though a few outliers did exist as explored in
695 the previous subsections. Overall, it is reassuring that the different methods yielded similar
696 results with most differences easily explained. This is the first work to examine these
697 relationships through multiple methods and compare them.
698 Application of this analysis to future research should probably be limited to using the

699 deepest craters method results when separated by terrain type. If a crater is emplaced in a terrain
700 that was not covered by the four major ones analyzed here, then researchers should use the
701 latitude bands. Using the global average will result in underestimating original crater depth in
702 some cases such as on volcanic terrain, or overestimating original depth in locations such as near
703 the poles.

704 6. The Simple/Complex Morphology Transition

705 Simple craters are small with concave floors while complex craters are large and have a
706 variety of interior morphologies such as wall terraces, central peaks, and flat floors.
707 Fundamentally, the transition diameter between simple and complex craters has been observed to
708 be a function of the surface gravity of the target object [e.g., *Baldwin*, 1949; *Quaide et al*., 1965;
709 *Malin and Dzurisin*, 1977; *Pike*, 1977, 1980a]. However, it is also at least in part controlled by
710 target material strength [e.g., *Pike*, 1980b, 1988]. Determining the diameter at which an impact
711 crater will transition from simple to complex morphology can inform studies of the target, its
712 properties, and the role of gravitational collapse and elastic rebound. These are the main
713 mechanisms during crater formation's modification phase that produce complex morphologies.
714 While the diameter of this transition is necessarily a range because different morphologies will
715 begin to form at different diameters, the diameter of this transition was found to be roughly 6 km
716 for Mars with no significant terrain dependence [*Pike*, 1988]. This value has been argued about
717 over the years with each new dataset of craters, and in that tradition this database was mined to
718 determine if Pike's [1988] synthesis requires revision.
719 In that spirit, this section examines four different types of simple-to-complex transitions –
720 basic floor morphology, onset of central peaks and terraces, and depth/Diameter transitions – for
721 the globe, latitude ranges, and terrain type. Any deviations from the canonical value have
722 implications for the surface material and can be used as a tracer for that.

723 6.1. Based on Floor Shape

A crater is considered to be within the basic complex type when it displays a flat floor morphology that is not due to post-formation infilling. Additional features are often characteristic of complex craters, but these are addressed in subsequent sections. Towards the goal of discerning the average diameter transition from simple to basic complex morphology, all craters in the database were classified from the available data - if possible - into these basic types. Craters in the ~4-8 km-diameter range were not classified if it was not clear if they were either fresh-appearing complex flat-floored craters or infilled (modified) simple craters (see *Robbins and Hynek*, 2012, this volume). It should be noted that simple craters were observed to be as large as D~13-14 km, but these were outliers and well above the average transition diameter calculated below.

Three histograms were created to quantify this: all craters, all simple craters, and all complex craters. The simple and complex crater histograms were then divided by the overall database histogram, and these are displayed in Fig. 12; the sum of the two is also shown. The simple-complex transition diameter is where the fraction of complex craters is greater than simple craters, and it is 6.9 km (Fig. 12). This diameter proved to be robust when separated into the two latitude ranges with the equatorial transition at 7.0 km and polar at 6.9 km. Examining craters at higher latitudes, however, yields interesting results: Poleward of ±60°, the transition occurs at 7.7 km, and at >±70°, it rises to 8.0 km (this is robust as there are still N>1000 craters). Separating these by northern and southern hemispheres yields a transition at 8.1 km for <-70°N, and those >+70°N have a transition ~8.4 km. A similar effect was found when separating by terrain type as in Section 5.2: Polar terrain craters had a transition of ~7.9 km while the other three (northern plains, southern highlands, and volcanic) were ~7.0 km. This is similar to findings by *Garvin et al*. [2000].

The dependence upon latitude and terrain has not been quantified before. As discussed, the transition is a consequence of collapse under gravity due to surpassing the strength of the target. (Impactor velocity will also play a role in this transition [*Pike*, 1988; *Schultz*, 1988], discussed in greater detail in section 6.4.) This runs contrary to what one would expect for the

751 Martian crust for, as graphically illustrated in Section 5, the higher latitudes of the planet are
752 likely dominated by a near-surface cryosphere [*Boynton et al*., 2002] and the cryosphere at
753 northern latitudes is probably closer to the surface (Section 5.2.2). From this, one would expect
754 an impact into an ice-solidified crust would vaporize volatiles and weaken the crust, permitting
755 gravitational collapse to a complex crater at smaller diameters rather than strengthening it for
756 transitions at larger diameters. One possible explanation is that water in the surface causes it to
757 act more fluid during the modification phase of crater formation, resulting in material gently
758 sloping down the crater walls, shallowing the bowl, but maintaining the bowl shape overall.
759 Another explanation is that infilling or general blanketing as a consequence of obliquity cycling
760 could account for some or all of this effect.

761 6.2. Simple-Complex Transition Based on Other Complex Crater Morphologies

762 Although *Pike* [1980b, 1988] examined several morphologies (flat floor (addressed
763 above), central peak, scalloped rim, terraced wall, ballistic ejecta, flow ejecta), in this analysis
764 the morphologies are limited to two additional ones – central peaks and terraced walls. Central
765 peaks form by rebound of the crust during crater formation [*e.g.*, *Wood*, 1973, *Roddy*, 1976].
766 Terraces are a collapse feature from the walls during crater formation; basic wall collapse, such
767 as talus, was not considered here. While these are fundamentally different processes, and they
768 will manifest at different crater sizes, they are each a good morphologic indicator of failure of
769 the crust to support a simple bowl and hence display a complex crater. Craters were binned
770 similarly as in the basic morphology, discussed above. An average was taken at the diameter
771 where the fraction of the craters that contained the feature was stable. Then, the diameter at
772 which 50% of the average was reached was considered the transition diameter.

773 Central peaks were present in an average of 6.3% for craters of all preservation states
774 with diameters $D \geq 15$ km. 50% of this was reached at $D = 5.6$ km. The smallest crater with a
775 central peak was ~2 km, but it did not reach 5% of the steady-state 6.3% level until $D \geq 3.3$ km.
776 The same analysis on equatorial craters shows a smaller diameter transition $D = 4.8$ km, while

777 the >±40° latitude range yielded a larger diameter of 11.3 km. Similar results were found on
778 volcanic and southern highlands terrain while there were not enough craters for an analysis on
779 polar deposits. The northern plains were significantly different with a transition to central peaks
780 at D = 8.4 km.

781 Terrace morphology did not reach a steady state until $D \approx 15$ km, and this was at a level
782 of 21%. 50% of this was reached at D = 8.3 km. The smallest crater with wall terraces was ~3
783 km, but it did not reach 5% of steady-state until $D \geq 4.5$ km. The same analysis on equatorial
784 craters shows a slightly smaller diameter transition of D = 7.5 km, while the >±40° latitude range
785 yielded a significantly larger transition diameter of 16.9 km. Terrain-dependent results were
786 similar to the global average except for polar where again small numbers made this analysis
787 difficult; the smallest diameter crater with visible terraces on polar terrain was 10 km.

788 These values are in rough agreement with *Pike* [1980b] who found transition diameter
789 from central peaks and terraces to be in the 6-8 km-diameter range with the prevalence of wall
790 terraces at larger diameters than central peaks (the worker found a difference of a factor of $2\times$,
791 though this work and methodology shows it to be $1.5\times$). The latitude range-dependent trend
792 observed here supports the idea from flat floor morphology that it is more likely this is a real
793 feature of the craters rather than an error in classification.

794 Issues with erosion of these more complex features are likely significant, for one would
795 expect the vast majority of larger complex craters form with terraced walls and likely central
796 peak features from basic cratering physics [*Melosh*, 1989]. For example, when only examining
797 fresh craters, terraces were identified in >90% of craters $D \geq 20$ km, and central peaks were
798 present in 55% of $8 < D < 13$ km craters and >90% of $D > 14$ km craters. However, we expect
799 that our ability to visually identify the presence of these features will be fairly uniform in the
800 ~10-20 km-diameter range despite erosion, and tests of examining hundreds of craters classified
801 as "pristine" showed comparable results.

802 6.3. Simple-Complex Transition Based on depth/Diameter

803 A more common method of determining transition diameter is on a crater depth versus
804 diameter plot (e.g., Fig. 13). On these, simple craters have a relatively steep slope compared
805 with complex craters, and there will be a slope discontinuity where they intersect. Some overlap
806 is present due to target, impactor, and other variances, but in general this occurs over a narrow
807 diameter range. When fitting the slopes to a power law function (Section 5.2), there is an exact
808 diameter at which the slopes intersect. This diameter is what is used and reported here.
809 Globally, for the deepest craters method, the transition diameter is 3.0 km. The fresh
810 crater method puts the transition at 5.9 km, while the all-crater average is 3.1 km. Transitioning
811 to the equatorial latitude band, the diameter goes down slightly for all cases - following the
812 pattern in the previous two sections - to 2.8 km, 4.4 km, and 2.9 km. The higher latitudes saw
813 mixed results with a spurious 9.2 km result for the deepest craters method due likely to small
814 numbers, 5.3 km for the fresh method, and 4.2 km for the global average. These values are also
815 considered to be similar and non-significant in terms of differences except in the higher latitudes
816 (see below). Overall, these are nearly all smaller than the simple-to-complex transition diameter
817 than when based upon morphology alone. This phenomenon was observed in previous work by
818 *Pike* [1988] not only on Mars, but also on Earth, Mercury, and the Moon. A figure similar to his
819 Fig. 11 is shown as Fig. 13, illustrating this point as well as showing the general diversity of the
820 onset of these morphologic and morphometric characteristics.

821 6.4. Synthesis of the Simple/Complex Morphology Transition
822 Overall, this is the first work to utilize a modern global crater database to examine the
823 simple-to-complex morphology transition on Mars. It does so with respect to multiple
824 morphologic and morphometric indicators and a latitude and terrain dependence. The results of
825 this analysis of independent morphologic and morphometric transitions are summarized in Fig.
826 14 and Table 3. Only the transition diameters for the deepest craters' d/D relationship are used to
827 calculate the arithmetic and geometric means (except for polar terrain). These means are very
828 close to each other, and the standard arithmetic would normally be used, but *Pike* [1988] used

829 geometric so that is included as a comparison. The means for the global distribution are 6.0 km
830 average and 5.6 km geometric; the standard deviation is ±2.3 km. *Pike* [1988] calculated ~6 km
831 for the transition. The other results are in Table 3.

832 This work supports Pike's [1980a, 1988] analysis from *Viking* images that found different
833 transition diameters for different simple/complex morphologies, as is indicated by the overlap
834 shown in Fig. 15. It is, however, significantly more robust, utilizing thousands of craters across
835 the globe instead of 230 craters. It used a variety of modification states as well as and only fresh
836 craters as a check. The global results fit very well within Pike's synthesis and lie directly upon
837 the lower dashed line of Fig. 15 that indicates similarity with sedimentary rock on Earth.
838 However, caution should be made in the interpretation of this figure, for impactor velocity will
839 play a role in this transition [*Pike*, 1988; *Schultz*, 1988] which can account for the failure of Mars
840 and Mercury to (a) be similar and (b) lie on the Earth-Moon line.

841 Of particular interest is the latitude and terrain dependence shown. This result was robust
842 in the previous sections: The equatorial range of <±40° latitude showed slightly smaller
843 diameter transitions while the polar latitude range had craters that transitioned at significantly
844 larger diameters for nearly all morphologic and morphometric indicators (though the ranges do
845 slightly overlap, as shown in Fig. 14). The implication is that crust type that dominates in the
846 equatorial band of Mars is less competent and craters will undergo gravitational collapse during
847 the modification phase of formation more readily. Meanwhile, the crust closer to the poles is
848 more competent and less prone to this form of collapse. Interestingly, this runs contrary to the
849 basic interpretation of crater depth/Diameter data discussed in Section 5. That indicated the crust
850 was weaker near the poles because even morphologically fresh craters were a factor of $\sim 2-3\times$
851 shallower than their equatorial counterparts. An alternative or additional explanation to
852 reconcile these could be that dusty deposits at high latitudes may prohibit slump blocks forming
853 at smaller sizes, causing the transition to complex morphology to be at larger diameters. These
854 disparate relationships are addressed in Section 7.

7. Discussion and Conclusions

We have explored the basic crater distributions, morphologic distributions, morphologic relationships, and morphometric relationships from a new global crater database of Mars. This database was shown to be statistically robust [*Robbins and Hynek*, 2012, this volume], and we examined many previously observed trends to illustrate and confirm its agreement with previous work. We also expanded the analysis to illustrate and confirm the utility in discerning new trends and relationships as well as to refine some that have been studied for decades.

In basic crater distribution across the planet, we showed that smaller diameters illuminate significant new work and forms the bulk of the number of craters in this database. The small crater population shows finer age variations across the surface in contrast with 5-50-km-diameter populations, and it also starts to inform studies of secondary crater populations [*Robbins and Hynek*, 2011a, 2011b].

Our work examining crater interior morphologies (central peaks, summit pits, and central pits) provides validation of our database, updates older results [e.g., *Barlow and Bradley*, 1990], and extends other modern ongoing work to the southern hemisphere [*Barlow*, 2010, 2011]. Central peak distribution generally correlates with fresh craters, but there is disagreement at central longitudes in the southern hemisphere. Further efforts in understanding this should be fruitful, as will further exploration into the distribution of Martian central pits and summit pits. The terrain in which these latter features are found supports a model that incorporates volatiles in their formation [e.g., *Wood et al*., 1978; *Croft*, 1981; *Senft and Stewart*, 2008; *Alzate and Barlow*, 2011], though the specific model is open to interpretation from our cursory analysis. Morphometric analysis may support this and is underway by other researchers [*Barlow*, 2010, 2011; *Alzate and Barlow*, 2011].

The distribution of radial ejecta was found to reproduce relative terrain ages reasonably well despite the craters forming after the terrain, illustrating that radial ejecta can be preserved over long periods of geologic time on Mars. Layered ejecta blanket data is abundant within the

881 database, comprising nearly 50% of the data columns [*Robbins and Hynek*, 2012, this volume,
882 Appendix A]. Extensive mining of these data for purposes of better explaining these features
883 and their formation is the subject of future work, but in this paper we showed its general
884 agreement with previous work in the area [e.g., *Mouginis-Mark*, 1979; *Schultz and Gault*, 1979;
885 *Barlow and Bradley*, 1990; *Barlow and Perez*, 2003; *Barlow*, 2005] and demonstrated its utility
886 in refining previous distributions and trends.

887 Our database provides detailed topographic information about craters, and this has
888 resulted in updating some of the empirical morphometric scaling laws as applied to Mars.
889 Overall, we found that Martian craters display rim morphometries that are $\sim 2\times$ smaller than
890 their lunar counterparts [summarized in *Melosh*, 1989]. This is the case for rim height and
891 surface-to-floor depth each relative to crater diameter, and these hold for both simple and
892 complex crater morphologies.

893 In further application to morphometric scaling, we examined the fresh-appearing crater
894 depth-to-diameter ratios (d/D) as an update to previously identified trends and values, though this
895 was the first analysis to compare three different methods from the same dataset for deriving the
896 d/D relationships on Mars. We illustrated the known global dichotomy of deeper craters in
897 equatorial regions and shallower craters towards the poles, and we expanded upon this to show a
898 previously unobserved secondary effect of a north/south dichotomy. This shows a wider
899 variation of crater depths towards the equator in the north compared with the south, but the
900 opposite was the case at polar latitudes. The high northern latitude craters showed a very tight
901 and shallow distribution of depths compared with the south, likely indicating a nearer surface
902 cryosphere and more uniform terrain. We reexamined the basic crater d/D relationship, as well,
903 for both the global average and subregions. Within each, we characterized d/D for simple and
904 complex craters in terms of the deepest craters, fresh craters, and all craters. Our results for the
905 global average compare well with previous work, and our results within the terrain dependence
906 reflect the dichotomy observed before. These differences are important, and they must be taken
907 into account when using crater depth to estimate erosion, infilling, and other modification

processes. Otherwise, there is the chance of interpreting all high-latitude craters as degraded relative to equatorial ones.

These *d*/*D* results for the deepest craters were then placed into the context of one of the other basic crater morphometric scaling laws in a method similar to what has been done in the past [e.g., *Pike*, 1977, 1980b, 1988]: At what diameter does a crater transition from simple to complex morphology? Three morphologic indicators were examined - basic morphology (bowl vs. flat floor), central peaks, and wall terraces - and the intersection of the *d*/*D* fits were our morphometric criterion. We again segregated by terrain as well as examined the global relationship. Our results agree very well with *Pike* [1988] for the global population, and this lends credibility to the incredible difference observed between latitude bands: We found the simple-complex transition occurs at ~11 km at high polar latitudes rather than the ~6 km global average (Fig. 14).

Taken with the *d*/*D* information for fresh and deep craters, we propose a model where the higher latitude craters will begin to form as they do elsewhere through the contact and excavation stage [*Melosh*, 1989]. During excavation, the impact energies will melt and vaporize ices in the nearby, surrounding crust (modeling indicates that more than enough ice would melt; see *Kraus and Stewart* [2010] or *Barr and Citron* [2011]). This will weaken the crust where vaporized, and intense ground movements cause the wet crust to flow like mud. During the modification phase, the crust is not strong enough to support the deep cavity characteristic of equatorial simple craters, but the viscous fluid-rich material will relax, decreasing the crater depth but maintaining a bowl shape. A central peak, generally the first complex morphologic indicator, does not form until $D \approx 11$ km poleward of ±40° and there were only two found in polar terrain. Either the central peak does not form in this suggested water-saturated crust until significantly larger diameters are reached, or it does form but quickly collapses and does not leave behind a visual indicator it existed.

The effect predicts that simple craters are maintained at larger diameters, but they are shallower than equatorial ones. This is more significant in high northern latitudes where there is

935 likely a nearer surface and/or thicker cryosphere [*Boynton et al*., 2002] enhancing this process.
936 This is supported by the cohesive layered ejecta morphology distribution found in the northern
937 hemisphere where their presence is also more prevalent than in the southern. The concentration
938 of DLE craters in high northern latitudes supports this, for it is likely that at least this type
939 requires a volatile in the subsurface to form based on the type's abundance over SLE on
940 Ganymede [*Boyce et al*., 2010], though it could also benefit from finer-grained silts, a lithology-
941 dependence [*Schultz*, 1992].
942 Overall, this new crater catalog with 384,343 craters $D \geq 1$ km is comparable to previous
943 ones where they overlap, and the additional morphologies and morphometries have proven to be
944 an unparalleled asset in studying the surface of Mars. This database freely available for
945 download via the Mars Crater Consortium section of USGS's PIGWAD server
946 (http://webgis.wr.usgs.gov/pigwad/down/mars_crater_consortium.htm). We have also made a
947 web-query site that allows users to download craters and features based on user-selectable fields
948 and options that is available at http://craters.sjrdesign.net.
949

950 Acknowledgements: The authors thank P.H. Schultz and S.C. Werner for thorough and helpful
951 reviews as well as the editors M. Wieczorek and D. Baratoux. S.J. Robbins thanks his
952 dissertation committee for feedback used to improve this work: F. Bagenal, N. Barlow, B.
953 Hynek, B. Jakosky, and N. Schneider. This work benefited from the assistance of R. Haber, D.
954 McKenzie, D. Russell, and K. Brugman. Support for this work was through NASA NESSF
955 Award NNX07AU85H and NASA Award NNX10AL65G.
956

957 References

958 Alzate, N., and N.G. Barlow (2011), Central pit craters on Ganymede, *Icarus 211*, 1274-1283,
959 doi: 10.1016/j.icarus.2010.10.015.

960 Baldwin, R.B. (1949), The Face of the Moon, University of Chicago Press, Chicago.

961 Banks, M.E., S., Byrne, K., Galla, A.S., McEwen, V.J., Bray, C.M., Dundas, K.E., Fishbaugh,
962 K.E., Herkenhoff, and B.C. Murray (2010), Crater population and resurfacing of the
963 Martian north polar layered deposits, *J. Geophys. Res.*, *115*, E08006, doi:
964 10.1029/2009JE003523.

965 Barlow, N.G. (1988), Crater size-frequency distributions and a revised Martian relative
966 chronology, *Icarus*, *75*, 285-305, doi: 10.1016/0019-1035(88)90006-1.

967 Barlow, N.G. (2005), A review of Martian impact crater ejecta structures and their implications
968 for target properties, in Kenkmann, T., F., Hörz, and A. Deutsch, eds. Large meteorite
969 impacts III: Geological Society of America Special paper *384*, 433-442.

970 Barlow, N.G. (2010), Central pit, central peak, and elliptical craters in the Martian northern
971 hemisphere: New results from the revised Catalog of Large Martian Impact Craters,
972 *Lunar Planet. Sci. Conf.*, *XLI*, Abstract #1065.

973 Barlow, N.G. (2011) Constraints on the proposed formation models for Martian central pit
974 craters, *Lunar Planet. Sci. Conf.*, *XLII*, Abstract #1149.

975 Barlow, N.G., J.M., Boyce, F.M., Costard, R.A., Craddock, J.B., Garvin, S.E.H., Sakimoto, R.O.,
976 Kuzmin, D.J., Roddy, and L.A. Soderblom, (2000), Standardizing the nomenclature of
977 Martian impact crater ejecta morphologies, *J. Geophys. Res.*, *105*, E11, 26,733-26,738,
978 doi: 10.1029/2000JE001258.

979 Barlow, N.G., and T.L. Bradley (1990), Martian impact craters: Correlations of ejecta and
980 interior morphologies with diameter, latitude, and terrain, *Icarus*, *87*, 156-179.

981 Barlow, N.G., and C.B. Perez (2003), Martian impact crater ejecta morphologies as indicators of
982 the distribution of subsurface volatiles, *J. Geophys. Res.*, *108*, E8, doi:
983 10.1029/2002JE002036.

984 Barr, A.C., and R.I. Ctron (2011), Scaling of melt production in hypervelocity impacts from
985 high-resolution numerical simulations, *Icarus*, *211*, 913-916, doi:
986 10.1016/j.icarus.2010.10.022.

987 Boyce, J.M., N.G., Barlow, P., Mouginis-Mark, and S. Stewart (2010), Rampart craters on
988 Ganymede: Their implications for fluidized ejecta emplacement, *Meteor. & Planet. Sci.*,
989 *45(4)*, 638-661, doi: 10.1111.j.1945-5100.2010.01044.x.

990 Boyce, J.M., and H. Garbeil (2007) Geometric relationships of pristine Martian complex impact
991 craters, and their implications to Mars geologic history, *Geo. Res. Lett.*, *34*, L16201, doi:
992 10.1029/2007GL029731.

993 Boyce, J.M., P., Mouginis-Mark, H., Garbeil, and L.L. Tornabene (2006), Deep impact craters in
994 the Isidis and southwestern Utopia Planitia regions of Mars: High target material strength
995 as a possible cause, *Geo. Res. Lett.*, *33*, L06202, doi: 10.1029/2005GL024462.

996 Boynton, W.V., and 24 colleagues, (2002), Distribution of hydrogen in the near surface of Mars:
997 Evidence for subsurface ice deposits, *Science*, *297*, 81-85, doi: 10.1126/science.1073722.

998 Bray, V.J., G.S., Collins, and J.V. Morgan (2006), Numerical modeling of impact cratering on

the Moon and icy satellites, *Lunar Planet Sci. Conf.*, *XXXVII*, Abstract #1175.

Byrne, S. and 17 colleagues (2009), Distribution of mid-latitude ground ice on Mars from new impact craters, *Science*, *325*, 1674-1676, doi: 10.1126/science.1175307.

Carr, M.H., L.S., Crumpler, J.A., Cutts, R., Greeley, J.E., Guest, H. and Masursky (1977), Martian impact craters and emplacement of ejecta by surface flow, *J. Geophys. Res*., *82(28)*, 4055-4065, doi: 10.1029/JS082i028p04055.

Chapman, C.R., and K.L. Jones (1977), Cratering and obliteration history of Mars, *Ann. Rev. Earth Planet. Sci.*, *5*, 515-540.

Christensen, P.R., and 10 colleagues (2004), The Thermal Emission Imaging System (THEMIS) for the Mars 2001 Odyssey Mission, *SSRv*, *110:1*, 85-130, doi: 10.1023/B:SPAC.0000021008.16305.94.

Clifford, S.M. (1993), A model for the hydrologic and climatic behavior of water on Mars, *J. Geophys. Res.*. *98(E6)*, 10,973,11016, doi: 10.1029/93JE00225.

Craddock, R.A., and T.A. Maxwell (1993) Geomorphic evolution of the Martian highlands through ancient fluvial processes, *J. Geophys. Res.*, *98(E2)*, 3453-3468, doi: 10.1029/92JE02508.

Croft, S.K. (1981), On the origin of pit craters, *Lunar Planet. Sci. Conf.*, *88*, 196-198.

Daubar, I.J., A.S., McEwen, S., Byrne, C.M., Dundas, A.L., Keske, G.L., Amaya, M., Kennedy, and M.S. Robinson (2011), New craters on Mars and the Moon. *Lunar Planet. Sci. Conf.*, *XLII*, Abstract #2232.

Edwards, C.S., K.J. Nowicki, P.R. Christensen, J. Hill, N. orelick, and K. Murray (2011), Mosaicking of global planetary image datasets: 1. Techniques and data processing for Thermal Emission Imaging System (THEMIS) multi-spectral data, *J. Geophys. Res.*, *116*, E10008, doi: 10.1029/2010JE003755.

Frey, H.V. (2008), Ages of very large impact basins on Mars: Implications for the late heavy bombardment in the inner solar system, *Geophys. Res. Lett.*, *35*, L13203, doi: 10.1029/2008GL033515.

Garvin, J.B., S.E.H., Sakimoto, and J.J. Frawley (2000), North Polar Region craterforms on Mars: Geometric characteristics from the Mars Orbiter Laser Altimeter, *Icarus*, *144*, 329-352, doi: 10.1006/icar.1999.6298.

Garvin, J.B., S.E.H., Sakimoto, and J.J. Frawley (2003), Craters on Mars: Geometric properties from gridded MOLA topography, *Int. Conf. on Mars*, *6*, Abstract #3277.

Golombek, M.P., and 10 colleagues (2006), Erosion rates at the Mars Exploration Rover landing sites and long-term climate change on Mars, *J. Geophys. Res.*, *111*, E12S10, 1-14, doi: 10.1029/2006JE002754.

Grant, J.A., and P.H. Schultz (1993), Degradation of selected Terrestrial and Martian impact craters, *J. Geophys. Res.*, *98(E6)*, 11,025-11,042, doi: 10.1029/93JE00121.

Greeley, R., J.H., Fink, D.E., Gault, and J.H. Guest (1982) Experimental simulation of impact cratering on icy satellites, in Morrison, D., ed., Satellites of Jupiter, University of Arizona Press, Tucson, 340-378.

Greeley, R., and J.E. Guest (1987), Geologic map of the eastern equatorial region of Mars, USGS Misc. Inv. Series Map I-1802-B.

1041 Greeley, R., N., Lancaster, L., Steven, and T. Peter (1992), Martian aeolian processes, sediments,
1042 and features, in Kieffer, H.H., B.M., Jakosky, C.W., Snyder, and M.S. Matthews, eds.,
1043 Mars, 730-766, ISBN 978-0816512577.

1044 Hale, W., and J.W. Head (1979), Central peaks in lunar craters: Morphology and morphometry,
1045 *Proc. Lunar Planet. Sci. Conf.*, *11*, 2623-2633, doi:

1046 Hamilton, V.E., P.R., Christensen, H.Y. McSween, Jr., and J.L. Bandfield (2003), Searching for
1047 the source regions of Martian meteorites using MGS TES: Integrating Martian meteorites
1048 into the global distribution of igneous materials on Mars, *Meteorit. & Planet. Sci.*, *38*,
1049 871-885.

1050 Head, J.W., J.F. Mustard, M.A. Kreslavsky, R.E. Milliken, and D.R. Marchant (2003), Recent
1051 ice ages on Mars, *Nature*, *426*, 797-802, doi: 10.1038/nature02114.

1052 Hoefen, T.M., R.N., Clark, J.L., Banfield, M.D., Smith, J.C., Pearl, and P.R. Christensen (2003),
1053 Discovery of olivine in the Nili Fossae region of Mars, *Science*, *203*, 627-630, doi:
1054 10.1126/science.1089647.

1055 Hynek, B.M., R.E. Arvidson, and R.J. Phillips (2002), Geologic setting and origin of Terra
1056 Meridiani hematite deposit on Mars, *J. Geophys. Res.*, *107:E10*, doi:
1057 10.1029/2002JE001891.

1058 Ivanov, B.A. (2001), Mars/Moon cratering rate ratio estimates, *Chron. & Evol. of Mars*, 96, 87-
1059 104.

1060 Jankowski, D.G., and S.W. Squyres (1992), Topography of impact craters in "softened" terrain
1061 on Mars, *Icarus*, *100*, 26-39, doi: 10.1016/0019-1035(92)90015-Y.

1062 Komatsu, G., G.G., Ori, S., Di Lorenzo, A.P., Rossi, and G. Neukum (2007), Combinations of
1063 processes responsible for Martian impact crater "layered ejecta structures" emplacement,
1064 *J. Geophys. Res.*, *112*, E06005, doi: 10.1029/2006JE002787.

1065 Kraus, R.G., and S.T. Stewart (2010), Impact induced melting and vaporization on icy planetary
1066 bodies, *Lunar Planet Sci. Conf.*, *XLI*, Abstract #2693.

1067 Laskar, J., A.C.M., Correia, M., Gastineau, F., Joutel, B., Levrard, and P. Robutel (2004), Long
1068 term evolution and chaotic diffusion of the insolation quantities of Mars, *Icarus*, *170*,
1069 343-364, doi: 10.1016/j.icarus.2004.01.005.

1070 Le Fuevre, M., and M.A. Wieczorek (2008), Nonuniform cratering of the terrestrial planets,
1071 *Icarus*, 197, 291-306, doi: 10.1016/j.icarus.2008.04.011.

1072 Lissauer, J.J., S.W., Squyers, and W.K. Hartmann (1988), Bombardment history of the Saturn
1073 system, *J. Geophys. Res.*, *93*, 13,776-13,804, doi: 10.1029/JB093iB11p13776.

1074 Malin, M.C., and 13 colleagues (2007), Context Camera investigation on board the Mars
1075 Reconnaissance Orbiter, *J. Geophys. Res.*, *112(E5)*, doi: 10.1029/2006JE002808.

1076 Malin, M.C., and D. Dzurisin (1977), Landform degradation on Mercury, the Moon, and Mars -
1077 Evidence from crater depth/diameter relationships, *J. Geophys. Res.*, *82(2)*, 376-388, doi:
1078 10.1029/JB082i002p00376.

1079 McCauley, J.F. (1973), Mariner 9 evidence for wind erosion in the equatorial and mid-latitude
1080 regions of Mars, *J. Geophys. Res.*, *78(20)*, 4123-4137, doi: 10.1029/JB078i020p04123.

1081 Mellon, M.T., and B.M. Jakosky (1995), The distribution and behavior of Martian ground ice
1082 during past and present epochs, *J. Geophys. Res.*, *100(E6)*, 11,781-11,799, doi:

10.1029/95JE01027.

Melosh, H.J. (1989), Impact cratering: A geologic process, Oxford University Press, New York.

Mouginis-Mark, P.J. (1979), Martian fluidized crater morphology: Variations with crater size, latitude, altitude, and target material, *J. Geophys. Res.*, *84(B14)*, 8011-8022, doi: 10.1029/JB084iB14p08011.

Mouginis-Mark, P.J., and J.N. Hayashi (1993), Shallow and deep fresh impact craters in Hesperia Planum, Mars, *Earth, Moon, & Plan.*, *61*, 1-20.

Mutch, P., and A. Woronow (1980) Martian rampart and pedestal craters' ejecta-emplacement: Coprates Quadrangle, *Icarus*, *41*, 259-268, doi: 10.1016/0019-1035(80)90009-3.

Neukum, G., and R. Jaumann (2004), HRSC: The High Resolution Stereo Camera of Mars Express, in Wilson, A., and A. Chicarro, eds., *ESA Special Publications*, *1240*, 17-35.

Nimmo, F., and K. Tanaka (2005), Early crustal evolution of Mars, *Annu. Rev. Earth Planet. Sci.*, *33*, 133-161, doi: 10.1146/annurev.earth.33.092203.122637.

Passey, Q.R., and E.M. Shoemaker (1982), Craters and basins on Ganymede and Callisto - Morphological indicators of crustal evolution, in Morrison, D., ed., Satellites of Jupiter, University of Arizona Press, Tucson, 379-434.

Pike, R.J. (1976), Crater dimensions from Apollo data and supplemental sources, *Moon*, *15*, 463-477, doi: 10.1007/BF00562253.

Pike, R.J. (1977), Apparent depth/apparent diameter relation for lunar craters, *Proc. Lunar. Sci. Conf.*, *8*, 3427-3436.

Pike, R.J. (1980a), Control of crater morphology by gravity and target type: Mars, Earth, Moon, *Proc. Lunar Planet. Sci. Conf.*, *11*, 2159-2189.

Pike, R.J. (1980b), Formation of complex impact craters: Evidence from Mars and other planets, *Icarus*, *43*, 1-19, doi: 10.1016/0019-1035(80)90083-4.

Pike, R.J. (1988), Geomorphology of impact craters on Mercury, 165-273, Chapter 8 in Vilas, F., Chapman, C.R., and Matthews, M.S., eds., 1988, Mercury, University of Arizona Press, ISBN 0-8165-1085-7.

Quaide, W.L., D.E., Gault, and R.A. Schmidt (1965), Gravitative effects on lunar impact structures, *Annals of the New York Academy of Sci.*, *123*, 563-572.

Robbins, S.J., and B.M. Hynek (2011a), Distant secondary craters from Lyot crater, Mars, and implications for the surface ages of planetary bodies, *Geo. Res. Lett.*, *38*, L05201, doi: 10.1029/2010GL046450.

Robbins, S.J., and B.M. Hynek (2011b), Secondary crater fields from 24 large primary craters on Mars: Insights into nearby secondary crater production, *J. Geophys. Res.*, in press, doi: 10.1029/2011JG003820.

Robbins, S.J., and B.M. Hynek (2012), A new global database of Mars impact craters ≥1 km: 1. Database creation, properties, and parameters, *J. Geophys. Res*., in press, doi: 10.1029/2011JE003966.

Roddy, D.J. (1976), High-explosive cratering analogs for bowl-shaped, central uplift, and multiring impact craters, *Proc. Lunar Planet. Sci. Conf.*, *7*, 3027-3056.

Salamunićcar, G., S. Lončarić, P., Pina, L., Bandeira, and J. Saraiva (2011), MA130301GT

1124 catalogue of Martian impact craters and advanced evaluation of crater detection
1125 algorithms using diverse topography and image datasets, *Planet. & Space Sci.*, *59*, 111-
1126 131, doi: 10.1016/j.pss.2010.11.003.

1127 Schultz, P.H. (1988), Cratering on Mercury: A Relook, 274-335, Chapter 9 in Vilas, F.,
1128 Chapman, C.R., and Matthews, M.S., eds., 1988, Mercury, University of Arizona Press,
1129 ISBN 0-8165-1085-7.

1130 Schultz, P.H. (1992) Atmospheric effects on ejecta emplacement, *J. Geophys. Res.*, *97(E7)*,
1131 11,623-11,662.

1132 Schultz, P.H., and D.E. Gault (1979), Atmospheric effects on Martian ejecta emplacement, *J.*
1133 *Geophys. Res.*, *84(B13)*, 7669-7687.

1134 Schultz, P.H., and A.B. Lutz (1988) Polar wandering of Mars, *Icarus*, *73*, 91-141, doi:
1135 10.1016/0019-1035(88)90087-5.

1136 Schultz, P.H., R.A., Schultz, and J. Rogers (1982), The structure and evolution of ancient impact
1137 basins on Mars, *J. Geophys. Res*., 87, B12, 9803-9820. doi: 10.1029/JB087iB12p09803.

1138 Scott, D.H., and K.L. Tanaka (1986), Geologic map of the western equatorial region of Mars,
1139 USGS Mic. Inv. Ser. Map I-1802-A.

1140 Searls, M.L., and R.J. Phillips (2007), Tectonics of Utopia Basin, Mars: Results from finite
1141 element loading models, *Lunar. Planet. Sci. Conf.*, *XXXVIII*, Abstract #1965.

1142 Senft, L.E., and S.T. Stewart (2008), Impact crater formation in icy layered terrains on Mars,
1143 *Meteor. & Planet. Sci.*, *43(12)*, 1993-2013, doi: 10.1111/j.1945-5100.2008.tb00657.x.

1144 Smith, D.E., and 23 colleagues (2001), Mars Orbiter Laser Altimeter: Experiment summary
1145 after the first year of global mapping on Mars, *J. Geophys. Res.*, *106*, 23,689-23,722, doi:
1146 10.1029/2000JE001364.

1147 Smith, P.H., and 35 colleagues (2009), H_2O at the Phoenix Landing Site, *Science*, *325*, 58-61,
1148 doi: 10.1126/science.1172339.

1149 Soderblom, L.A., C.D., Condit, R.A., West, B.M., Herman, and T.J. Kreidler (1974), Martian
1150 planetwide crater distributions: Implications for geologic history and surface processes,
1151 *Icarus*, *22*, 239-263, doi: 10.1016/0019-1035(74)90175-4.

1152 Soderblom, L.A., T.J., Kreidler, and H. Masubsky (1973) Latitudinal distribution of a debris
1153 mantle on the Martian surface, *J. Geophys. Res.*, *78(20)*, 4117-4122, doi:
1154 10.1029/JB078i020p04117.

1155 Stepinski, T.F., M.P., Mendenhall, and B.D. Bue (2009), Machine cataloging of impact craters
1156 on Mars, *Icarus*, *203*, 77-87, doi: 10.1016/j.icarus.2009.04.026.

1157 Stewart, S.T., and G.J. Valiant (2006), Martian subsurface properties and crater formation
1158 processes inferred from fresh impact crater geometries, *Meteor. & Planet. Sci.*, *41(10)*,
1159 1509-1537.

1160 Strom, R.G., S.K. Croft, and N.G. Barlow (1992), The Martian impact cratering record, 383-423,
1161 Chapter 12 in Kieffer, H.H., Jakosky, B.M., Snyder, C.W., and Matthews, M.S., eds.,
1162 1992, Mars, University of Arizona Press, ISBN 0-8165-1257-4.

1163 Tanaka, K.L. (1986), The stratigraphy of Mars, *J. Geophys. Res.*, *91*, E139-E158, doi:
1164 10.1029/JB09liB13p0E139.

1165 Tanaka, K.L. (2000), Dust and ice deposition in the Martian geologic record, *Icarus*, 144, 254-

266, doi: 10.1006/icar.1999.6297.

Tanaka, K.L., J.M., Dohm, C.M., Fortezzo, R.P., Irwin, III, E.J., Kolb, J.A., Skinner, Jr., T.M., Hare, T., Platz, and S.J. Robbins (2012), The geology of Mars: What the new global map shows. *Lunar Planet. Sci. Conf.*, *XLIII*, Abstract #2702.

Tanaka, K.L., and D.H. Scott (1987), Geologic map of the polar regions of Mars, USGS Misc. Inv. Ser. Map I-1802-C.

Werner, S.C. (2008), The early Martian evolution - Constraints from basin formation ages, *Icarus*, *195*, 45-60, doi: 10.1016/j.icarus.2007.12.008.

Wood, C.A. (1973), Moon: Central peak heights and crater origins, *Icarus*, *20:4*, 503-506, doi: 10.1016/0019-1035(73)90023-7.

Wood, C.A., and L. Andersson (1978), Lunar Crater Morphometry: New data, *Lunar Planet Inst. Tech. Report*, *9*, 1267-1269.

Wood, C.A., J.W., Head, and M.J. Cintala (1978), Interior morphology of fresh Martian craters: The effects of target characteristics, *Proc. Lunar Planet. Sci. Conf.*, *9*, 3691-3709.

Woronow, A., and P. Mutch (1980), On the origin of Martian pedestal, lobate, and multilobate ejecta deposits, *Lunar Planet. Sci. Conf.*, *XI*, 1282-1284.

Zuber, M.T., D.E., Smith, S.C., Solomon, D.O. Muhleman, J.W., Head, J.B., Garvin, J.B., Abshire, and J.L. Bufton (1992), The Mars Observer laser altimeter investigation, *J. Geophys. Rev.*, *97*, 7781-7797.

1186 Table 1: Average ejecta mobility values for select layered ejecta types. Units are crater radii.

	SLE	DLE Inner	DLE Outer
Global	1.4	1.4	2.5
<-40°N Latitude	1.6	1.5	2.5
±30° Latitude	1.2	1.2	1.8
>+40°N Latitude	2.0	1.5	3.2

1187

Table 2**:** Crater depth/Diameter ratios on Mars have been quoted as overall global averages for decades, but examination of the global distribution shows there are variations based on terrain. This table shows the simple (top line) and complex (bottom line) depth/Diameter relationship when are divided into a variety of terrain types. The number *N* of craters in this table is the number used in the "All Craters" analysis.

		Deepest Craters	Fresh Craters	All Craters
Global	Smp (*N* = 37,091):	$d = 0.179D^{1.012}$	$d = 0.097D^{1.061}$	$d = 0.047D^{1.284}$
	Cpx (*N* = 32,021):	$d = 0.286D^{0.582}$	$d = 0.250D^{0.527}$	$d = 0.107D^{0.559}$
-40° to +40°	Smp (*N* = 24,875):	$d = 0.175D^{1.022}$	$d = 0.084D^{1.245}$	$d = 0.078D^{1.106}$
	Cpx (*N* = 22,290):	$d = 0.280D^{0.570}$	$d = 0.229D^{0.567}$	$d = 0.155D^{0.464}$
≤-40°, ≥+40°	Smp (*N* = 12,210):	$d = 0.177D^{0.724}$	$d = 0.083D^{1.073}$	$d = 0.014D^{1.465}$
	Cpx (*N* = 9742):	$d = 0.244D^{0.579}$	$d = 0.174D^{0.629}$	$d = 0.032D^{0.881}$
Northern Plains	Smp (*N* = 3693):	$d = 0.165D^{1.094}$	$d = 0.073D^{1.311}$	$d = 0.011D^{1.992}$
	Cpx (*N* = 1308):	$d = 0.479D^{0.359}$	$d = 0.274D^{0.502}$	$d = 0.227D^{0.158}$
Volcanic Terrain	Smp (*N* = 2471):	$d = 0.212D^{0.886}$	$d = 0.182D^{0.718}$	$d = 0.091D^{1.010}$
	Cpx (*N* = 1008):	$d = 0.291D^{0.526}$	$d = 0.240D^{0.539}$	$d = 0.209D^{0.451}$
Southern Highlands	Smp (*N* = 23,087):	$d = 0.235D^{0.777}$	$d = 0.154D^{0.821}$	$d = 0.051D^{1.261}$
	Cpx (*N* = 23,850):	$d = 0.303D^{0.571}$	$d = 0.231D^{0.556}$	$d = 0.112D^{0.541}$
Polar Terrain	Smp (*N* = 727):	–	–	$d = 0.0028D^{1.843}$
	Cpx (*N* = 202):	–	–	$d = 0.014D^{1.161}$

1194 Table 3**:** Summary of transitional diameters for different Martian terrains and derived through
1195 various means discussed in the text (all units are km).

	Global	<±40°	>±40°	S. High	N. Plains	Volcanic	Polar
Floors	6.9	7.0	6.9	7.0	7.2	7.0	7.9
C. Peak	5.6	4.8	11.3	5.2	8.4	5.3	–
Terr.	8.3	7.5	16.9	8.6	8.0	8.9	10.0
d/*D*, Deep	3.0	2.8	9.2	3.4	4.3	2.4	10.4[1]
A. Mean	6.0	5.5	11.1	6.1	7.0	5.9	9.4
G. Mean	5.6	5.2	10.5	5.7	6.8	5.3	9.4
Std. Dev.	2.3	2.2	4.3	2.2	1.9	2.8	1.3

1196 [1]There were not enough craters to derive a reliable function for the "deepest" crater method for
1197 polar terrain craters. The "all-craters" method value is quoted in its stead, and it was used to
1198 compute the averages and standard deviation.
1199

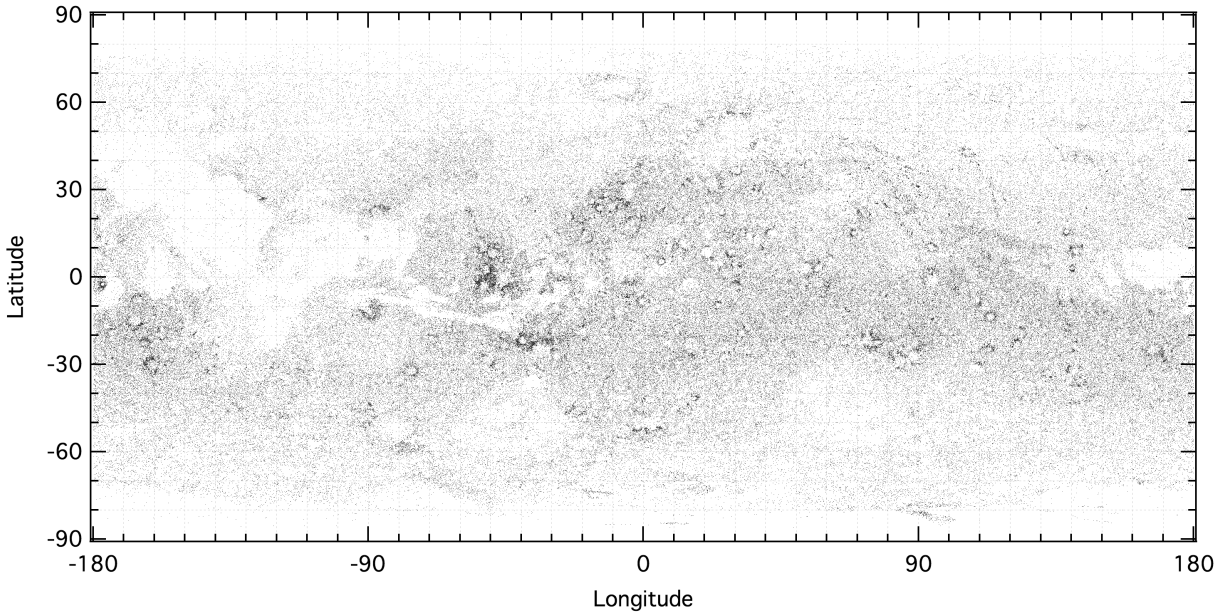

1200

1201 Figure 1: Locations of all $1 \leq D < 3$ km craters on Mars included in this database, including
1202 potential secondary craters.

1203

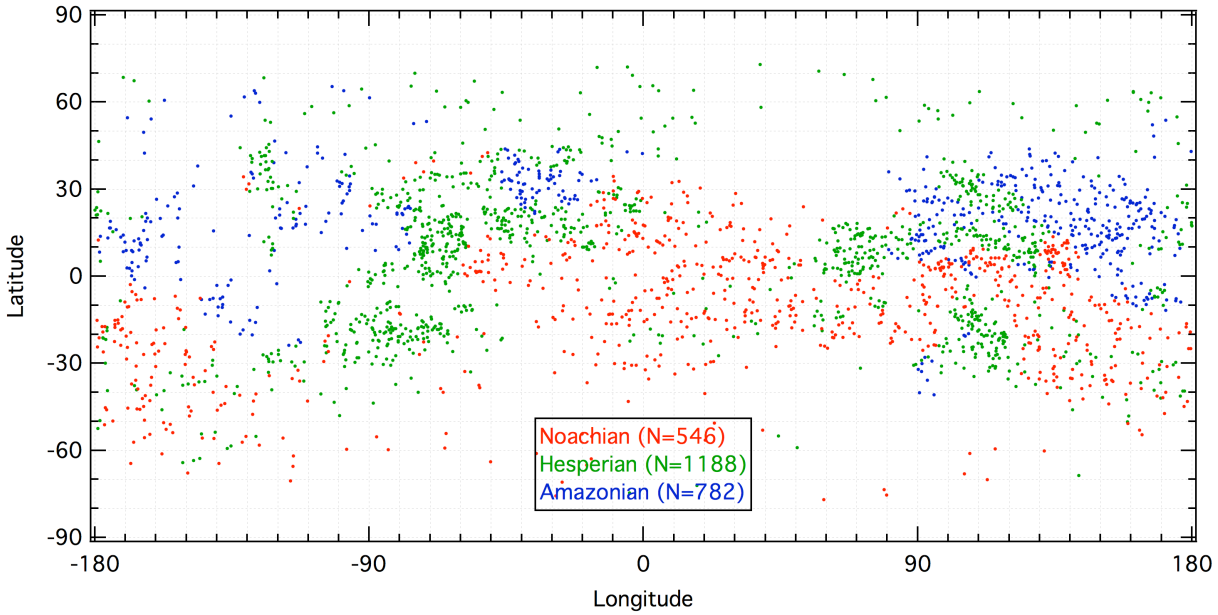

Figure 2**:** Scatter plot showing the distribution of all fresh $D \geq 5$ km fresh craters. Fresh craters are generally concentrated close to the equator but show a larger latitude range centered at ~200°E. Red dots represent craters on Noachian terrain, green are Hesperian, and blue are Amazonian. Terrain ages are from the Mars geologic maps [*Scott and Tanaka*, 1986; *Greeley and Guest*, 1987].

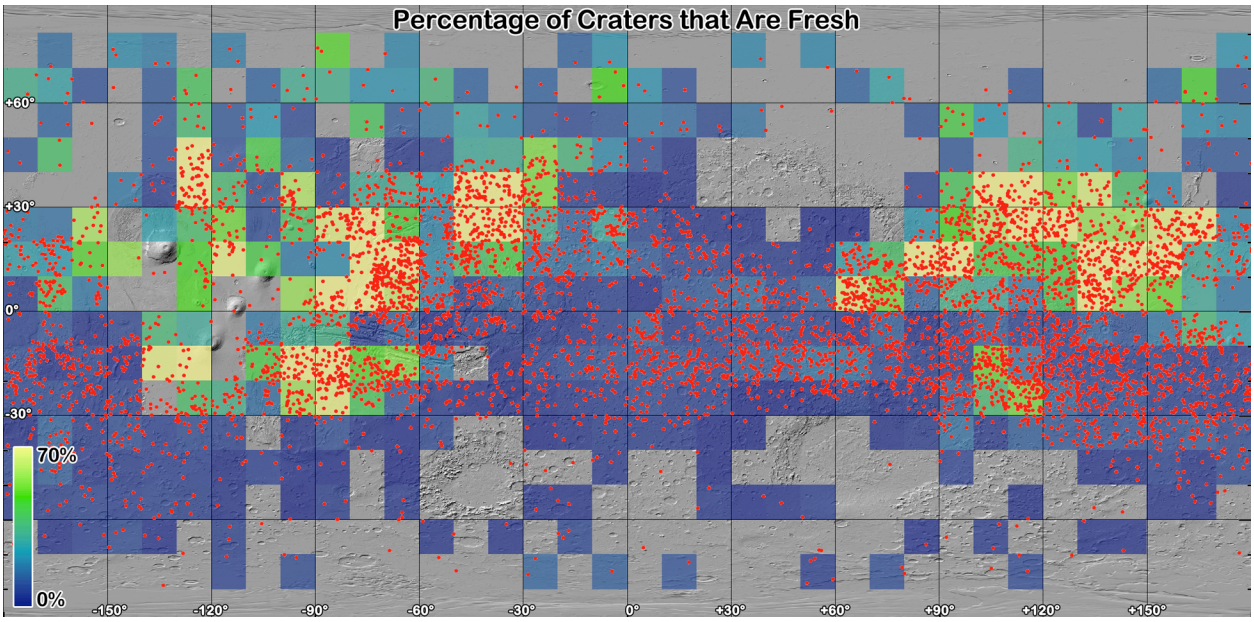

Figure 3**:** Area density plot showing the relative fraction of craters in 10°x10° bins that are fresh versus the population of all 5-50-km-diameter craters. The raw craters are shown as red dots. Gaps are where there were not enough craters for an analysis or there were 0% fresh craters. Graticules are 30°.

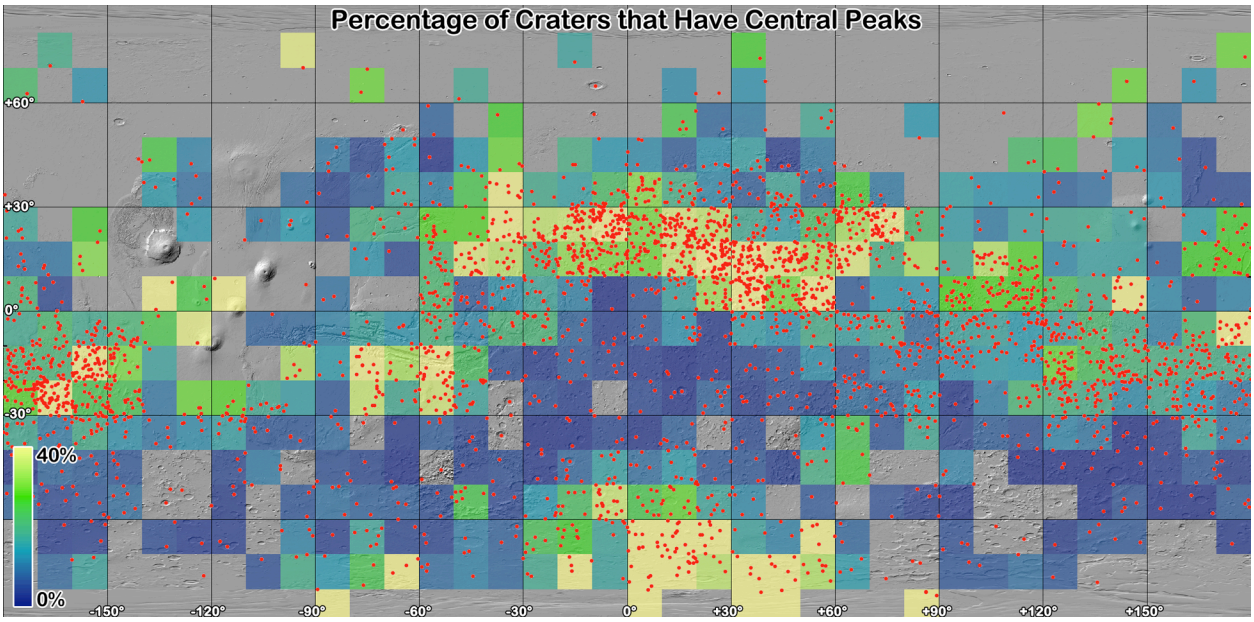

Figure 4**:** The fraction of craters $5 \leq D \leq 50$ km in 10°x10° bins that have central peaks. Underlying image is MOLA shaded relief. The raw craters are shown as red dots. Gaps are where there were no craters, graticules are 30°x30°.

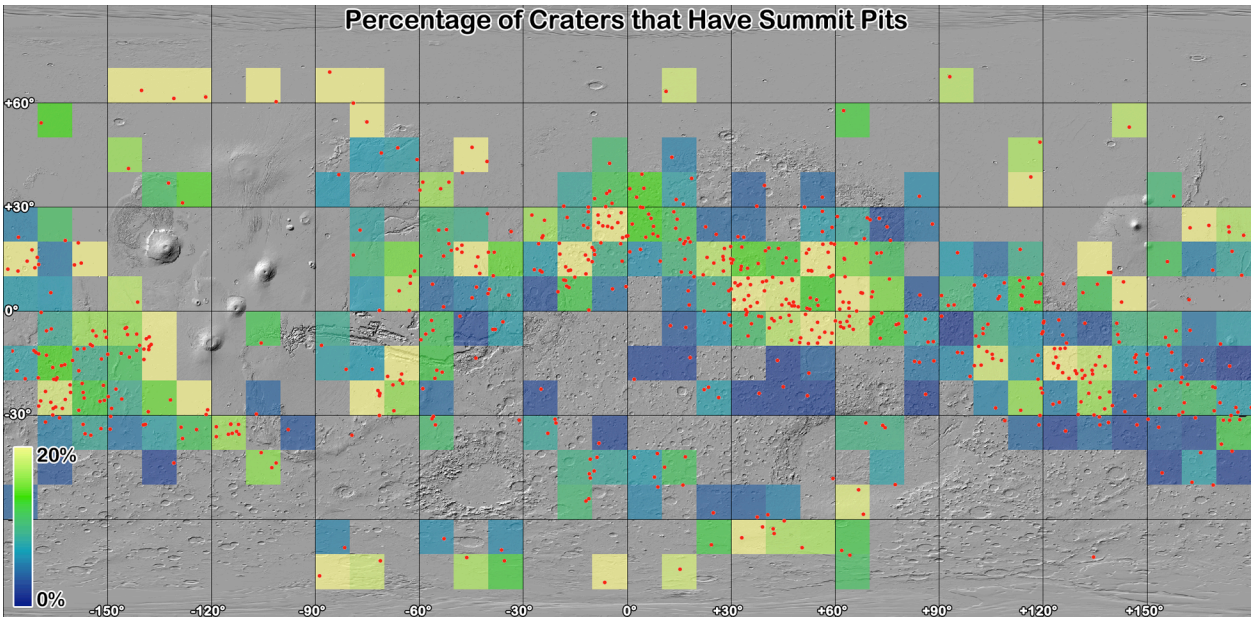

Figure 5**:** The fraction of craters 5≤*D*≤50 km in 10°x10° bins that have summit pits. Underlying image is MOLA shaded relief. The raw craters are shown as red dots. Gaps are where there were no craters, graticules are 30°x30°.

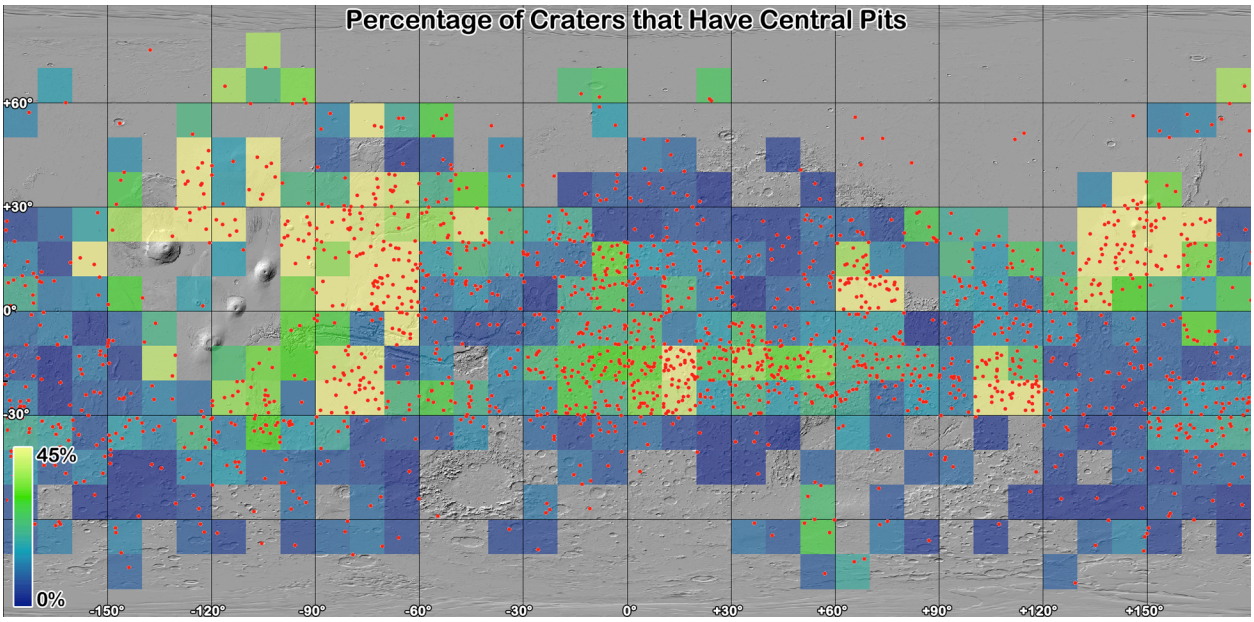

Figure 6**:** The fraction of craters $5 \leq D \leq 50$ km in 10°x10° bins that have central pits. Underlying image is MOLA shaded relief. The raw craters are shown as red dots. Gaps are where there were no craters, graticules are 30°x30°.

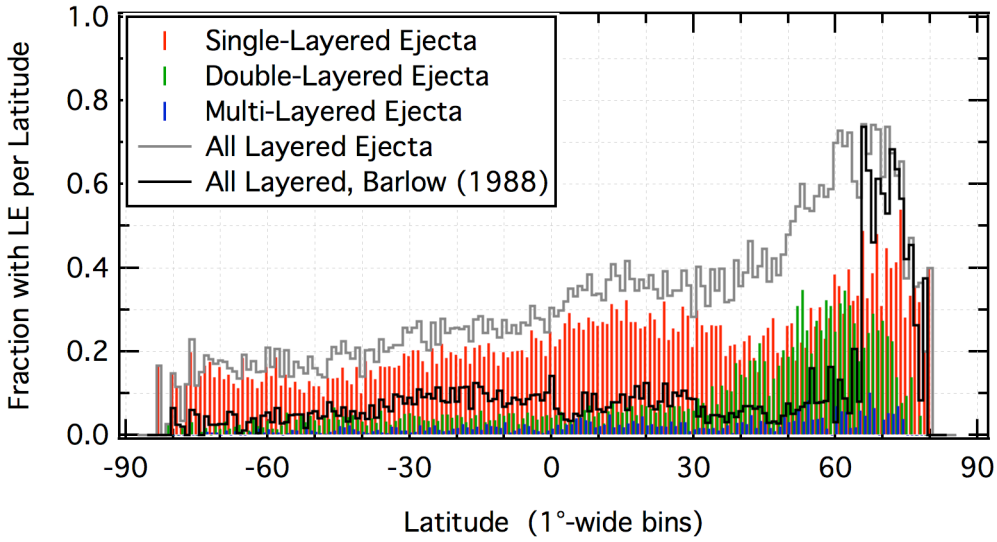

Figure 7**:** Distribution of layered ejecta craters, by type, per latitude bin for craters $D \geq 5$ km (for fair comparison with *Barlow* [1988]). Red, green, and blue indicate SLE, DLE, and MLE distribution, respectively, while the grey line shows the sum of all three. For reference, the sum of all LE types from *Barlow* [1988] is shown as a black line.

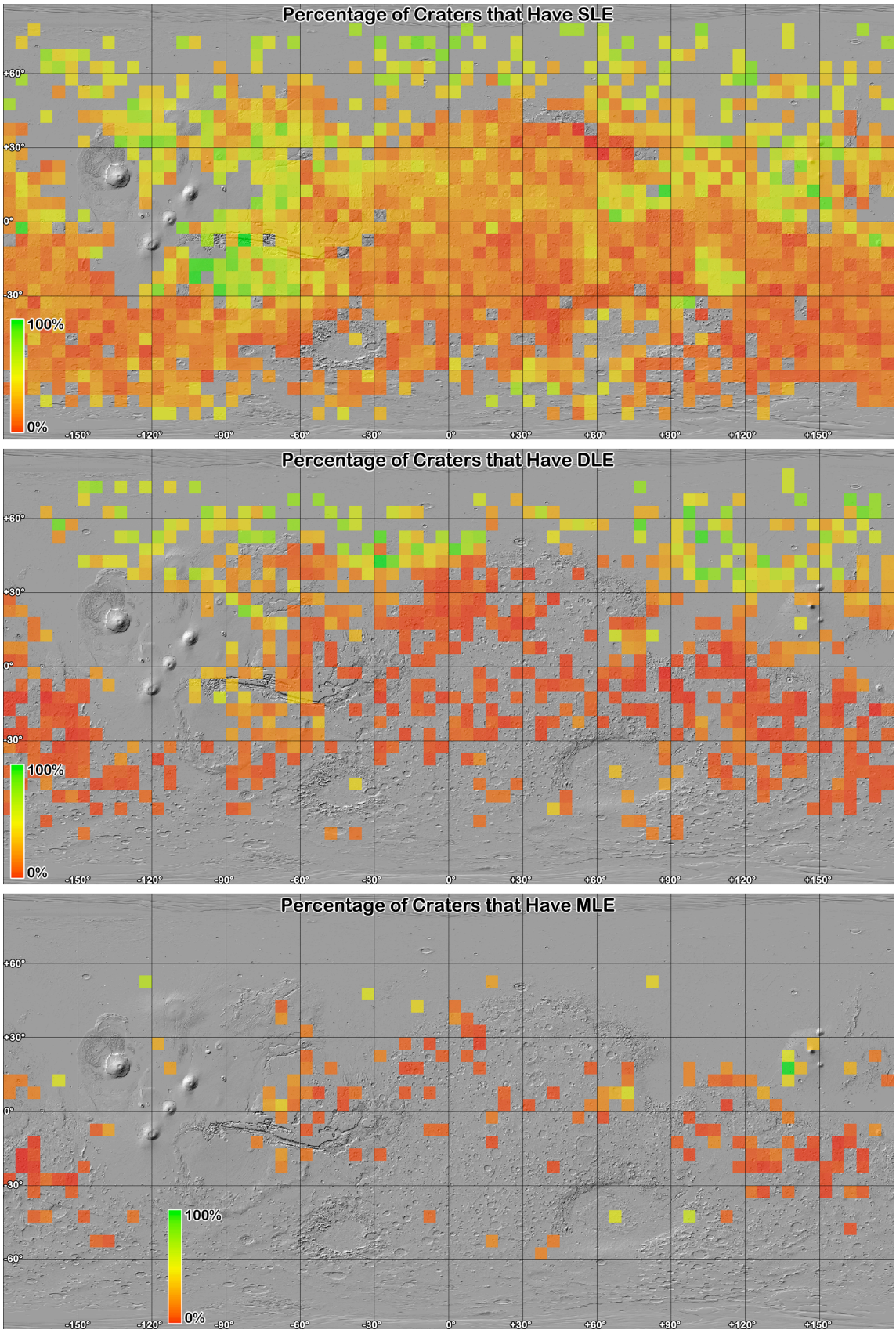
Percentage of Craters that Have SLE
+60°
+30°
0°
-30°
100%
0%
-150°
-120°
-90°
-60°
-30°
0°
+30°
+60°
+90°
+120°
+150°
Percentage of Craters that Have DLE
+60°
+30°
0°
-30°
100%
0%
-150°
-120°
-90°
-60°
-30°
0°
+30°
+60°
+90°
+120°
+150°
Percentage of Craters that Have MLE
+60°
+30°
0°
-30°
-60°
100%
0%
-150°
-120°
-90°
-60°
-30°
0°
+30°
+60°
+90°
+120°
+150°

1238

1239 Figure 8**:** The fraction of craters $5 \leq D \leq 50$ km in 5°x5° bins that have layered ejecta blankets.
1240 Underlying image is MOLA shaded relief. Gaps are where there were ≤1 craters of any type per
1241 bin, graticules are 30°x30°.
1242

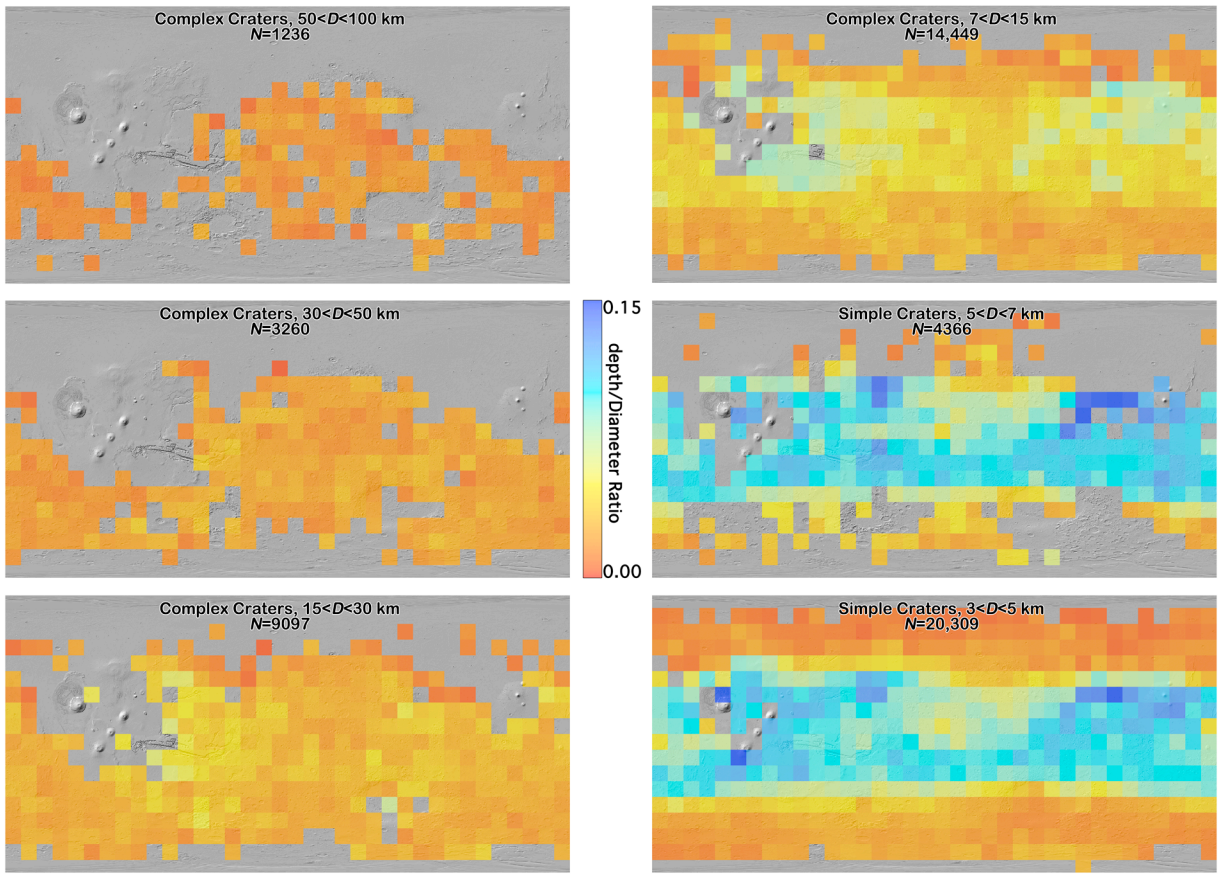

Figure 9**:** Six panels showing binned crater depth/Diameter ratios across Mars in 10°x10° bins; bins with $N < 5$ craters were removed. Four panels show complex craters and two are simple.

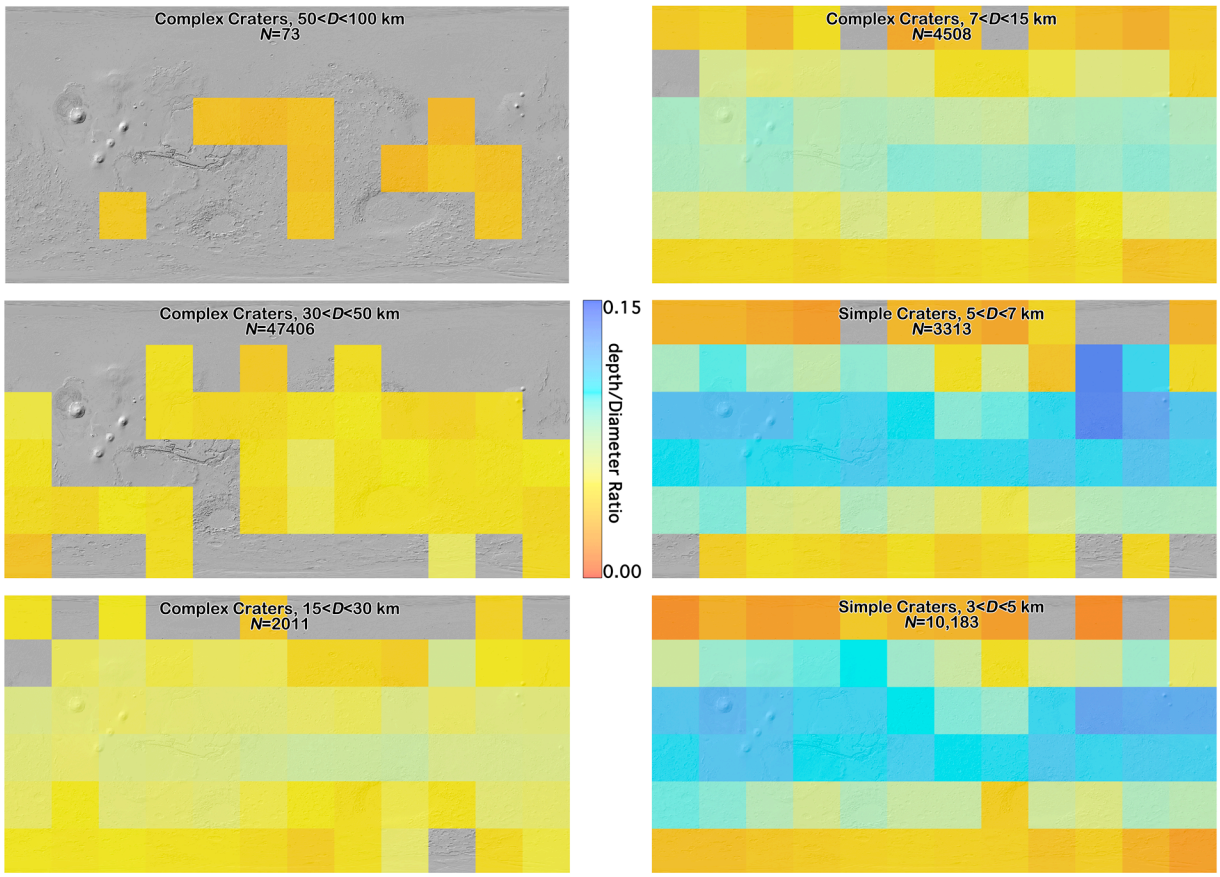

Figure 10**:** Six panels showing binned fresh (degradation states 3 and 4) crater depth/Diameter ratios across Mars in 30°x30° bins; bins with $N < 5$ craters were removed. Four panels show complex craters and two are simple.

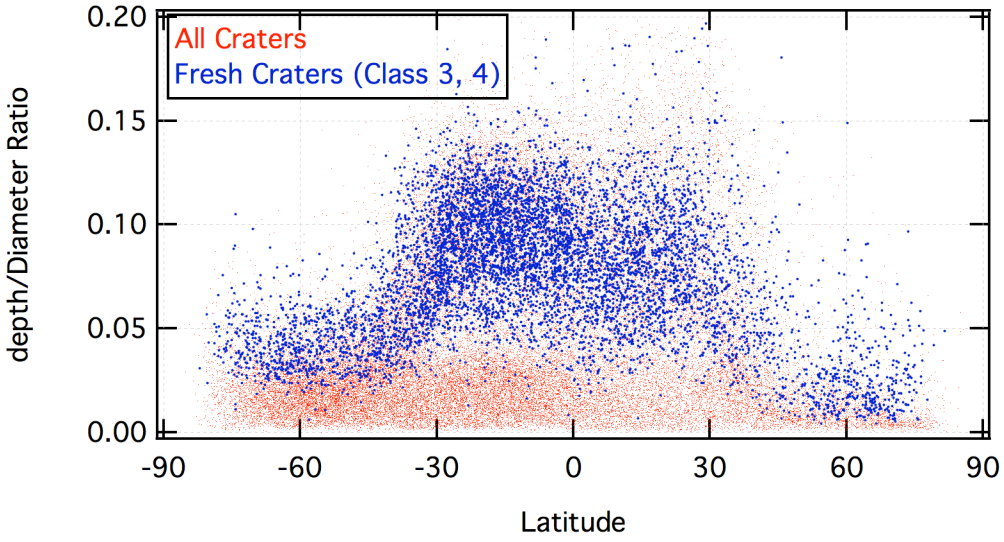

1252

1253 Figure 11: Scatter plot showing all craters with only fresh craters (preservation states 3 and 4)
1254 over-plotted. Red dots represent all craters and blue symbols are fresh craters.

1255

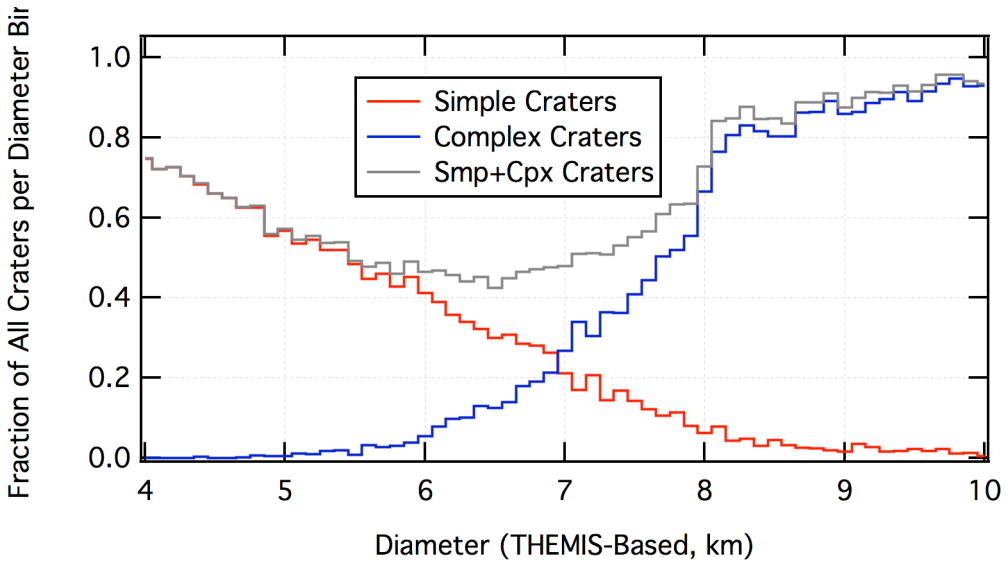

Figure 12**:** Three histograms were created as a function of diameter: All craters, simple craters, and complex craters. The simple and complex crater histograms were divided by the histogram for all craters and are plotted here, their sum shown in grey. The deficit relative to 100% of all craters being classified between ~5-8 km is due to the conservative classification to avoid classifying infilled simple craters as flat-floored pristine complex craters and vice-versa.

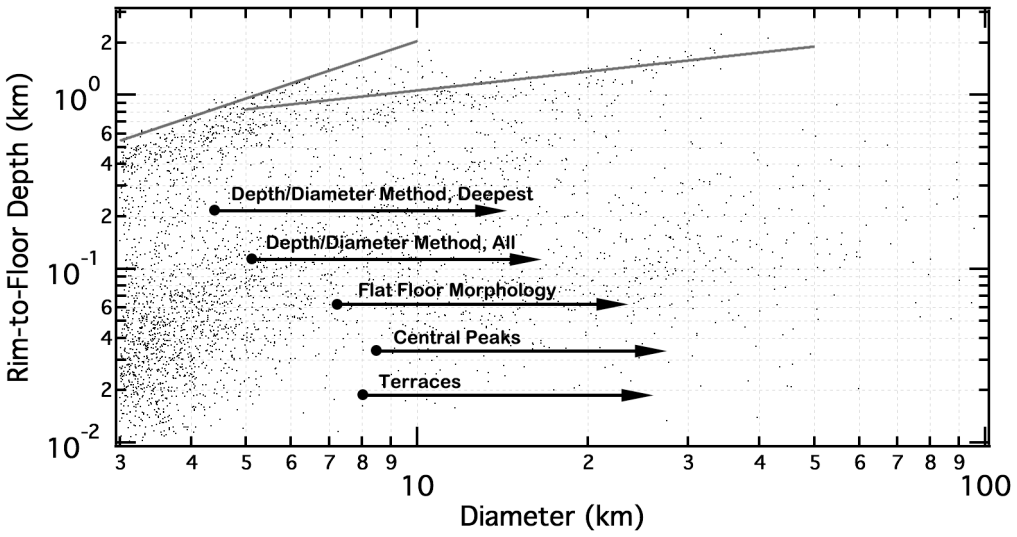

1263

1264 Figure 13**:** Simplified diagram illustrating the diameter at which the simple-complex transitions
1265 are observed for the northern plains. Dots are craters, and the two nearly crossing lines are the
1266 best-fits for simple and complex deep craters. Arrows indicate the transition diameter from
1267 simple to complex for each of the labeled characteristics examined (vertical offset is arbitrary).

1268

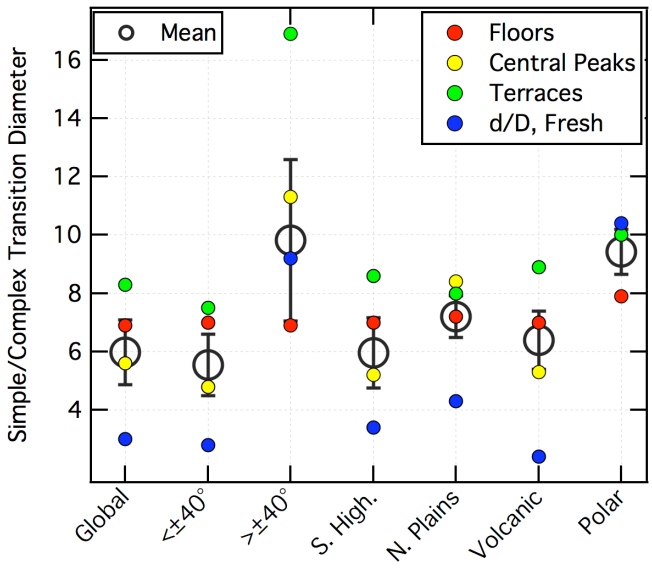

Figure 14**:** Combined results from using different morphologic and morphometric indicators to determine the transition between simple and complex crater morphology on Mars. Solid circles are points showing each result discussed in the text, the key to which shown by the legend to the upper right. Black open circles are the arithmetic means for all morphologic data and results from the deep crater *d*/*D* method (since that is considered the most robust technique (see Sections 5.2 and 5.3)). Error bars are the standard deviation from the means of the three or four values divided by $\sqrt{N}$.

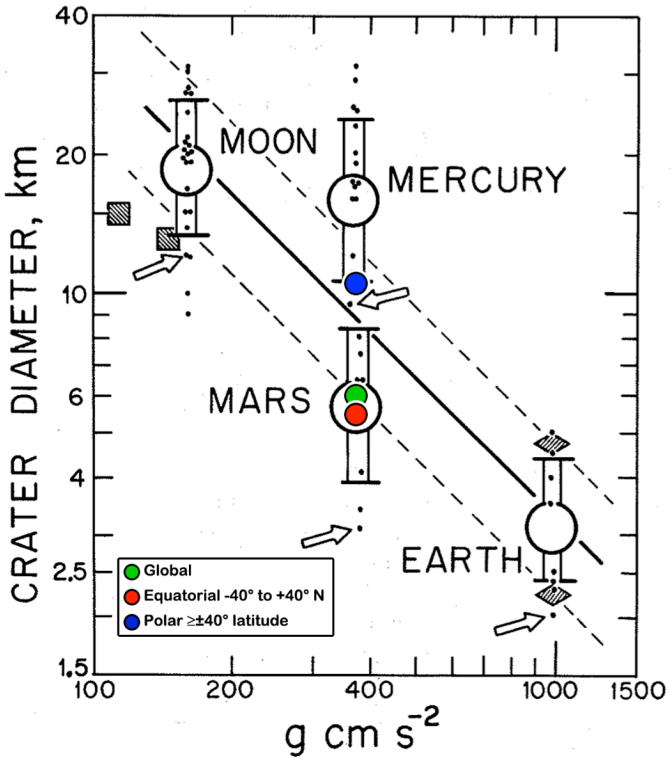

Figure 15: Background Figure is adapted from *Pike* [1988, used with permission, ©1989 The Arizona Board of Regents, University of Arizona Press], illustrating surface gravity versus onset of complex crater morphology for the large inner solar system bodies (except Venus) and Ganymede and Callisto (squares). Each small black dot is from *Pike* [1988] and represents a different morphologic indicator of this transition. Arrows point to *d*/*D* results in the original *Pike* [1988]. Large circles are geometric means and bars are standard deviations. The solid black line is a best-fit, while the diamonds are for different targets on Earth and the dashed lines extrapolations of the fit for those targets (lower is for sedimentary rock, upper is igneous). Overplotted in color are the results from this work (arithmetic means).